Coordinated Multi-Point Transmissions Based on Interference Alignment and Neutralization

Zhao Li, *Member, IEEE*, Jie Chen, Lu Zhen, Sha Cui, Kang G. Shin, *Life Fellow, IEEE*, and Jia Liu, *Member, IEEE*

***Abstract*— Both interference alignment (IA) and interference neutralization (IN) are exploited for coordinated multi-point (CoMP) communications. With the cooperation of the base station (BS), a transmit precoder and a receive filter are jointly designed, and concurrent transmissions of multiple data streams are then enabled. In the design of a precoder, the IN is applied to the interferences carrying the same data so as to align the interfering signals in the opposite direction in a subspace. On the other hand, for interferences carrying different information, IA is employed to align them in the same direction in a subspace, thus reducing the interference signal observed at the receiver side. Based on different precoding schemes at the transmitter's side, receivers adopt zero forcing (ZF) so as to recover the desired data. The proposed IA- and IN-based CoMP (IAN-CoMP) mechanism can achieve effective interference cancellation and suppression by exploiting limited and flexible collaboration at the BS side. It can also make a flexible tradeoff between the cooperation overhead and the system's achievable degrees of freedom (DoFs). We extend the mechanism to general cases where the antenna configurations at both the transmitter and receiver sides, the number of transmitters participating in CoMP, and that of simultaneously served users are variable. Moreover, we discuss both single-location and multi-location-based realizations of the IAN-CoMP. Finally, by defining the average transmit and receive cooperation order, we analyze the upper bound for IAN-CoMP. Our in-depth simulation shows that the IAN-CoMP can significantly improve the spectral efficiency (SE) for cell-edge users.**

***Index Terms*— Interference neutralization, interference alignment, coordinated multi-point (CoMP).**

Manuscript received May 13, 2017; revised November 16, 2017, May 12, 2018 and September 22, 2018; accepted March 18, 2019. Date of publication April 18, 2019; date of current version July 10, 2019. This work was supported in part by the China 111 Project under Grant B16037, in part by the Fundamental Research Funds for the Central Universities under Grant JB171503, in part by NSFC under Grant 61672410 and Grant 61802292, in part by the Project of Cyber Security Establishment with Inter University Cooperation, in part by the Secom Science and Technology Foundation, and in part by the U.S. National Science Foundation under Grant CNS-1317411. The associate editor coordinating the review of this paper and approving it for publication was O. O. Koyluoglu. *(Corresponding author: Zhao Li.)*

Z. Li is with the School of Cyber Engineering, Xidian University, Xi'an 710126, China, also with the Shaanxi Key Laboratory of Information Communication Network and Security, Xi'an University of Posts and Telecommunications, Xi'an 710121, China, and also with the School of Information Engineering, Eurasia University, Xi'an 710065, China (e-mail: zli@xidian.edu.cn).

J. Chen, L. Zhen, and S. Cui are with the School of Telecommunications Engineering, Xidian University, Xi'an 710071, China.

K. G. Shin is with the Department of Electrical Engineering and Computer Science, University of Michigan, Ann Arbor, MI 48109-2121 USA.

J. Liu is with the Center for Cybersecurity Research and Development, National Institute of Informatics, Tokyo 101-8430, Japan.

Color versions of one or more of the figures in this paper are available online at http://ieeexplore.ieee.org.

Digital Object Identifier 10.1109/TWC.2019.2908159

I. Introduction

IMPROVING spectral efficiency (SE) to meet the rapidly growing demand for high-speed data transmission is of great importance to wireless communication service providers [1]. In particular, as the frequency reuse efficiency improves, cell-edge users suffer more co-channel interference (CCI) from adjacent cells, which degrades the overall system performance. Interference has become the main impediment in cellular communications [2]. It is, therefore, critically important to effectively manage interference so as to solve the interference problem for cell-edge users and improve the system throughput [3]. Coordinated multi-point (CoMP) transmission—designed to solve the problem by enforcing the cooperation of multiple cells—is a promising technique and has been chosen as a key technology in the 3rd Generation Partnership Project (3GPP) long-term evolution-advanced (LTE-A) systems [2], [4]. CoMP was proposed to enable multiple BSs to jointly transmit data to multiple terminals, effectively exploiting interference to achieve large gains in SE and fairness. In particular, cooperation of multiple BSs (i.e., CoMP) is attractive since it improves the cell-edge data rate and average data rate, and is suitable to enhance SE (and hence capacity) for much more dense network deployments in urban areas and capacity hotspots [2]. Reference [2] provides a comprehensive overview of various CoMP techniques and [3] covers an information-theoretic approach to managing interference in future-generation wireless networks, focusing on cooperative schemes of CoMP.

Besides CoMP, there are other types of interference management, such as zero-forcing (ZF) [5]–[7] and interference alignment (IA) [8]–[12]. Using these, a set of BSs jointly encode the transmitted symbols, so that interference at the receiver may be effectively suppressed or mitigated, and then the desired signal is recovered accurately. Thanks to its simplicity, ZF-based precoding has been widely applied to CoMP systems [5]–[7]. A hybrid cooperative downlink transmission and preprocessing scheme that incorporates joint processing (JP) and coordinated scheduling/beamforming (CS/CB), was proposed in [5] for heterogeneous networks. A low-feedback scheduling scheme was proposed in [6] for downlink CoMP systems, in which multiple users are selected and then served simultaneously with zero-forcing beamformer by several cooperative BSs. A dynamic switching mechanism between CoMP mode and non-CoMP mode was proposed

in [7] to adapt to a dynamically changing communication environment.

IA is a novel interference management that has been under development in recent years [8]–[12]. By preprocessing at the transmitter, multiple interfering signals are mapped into a finite subspace, i.e., the overall interference space at the destination/receiver is minimized, so that the desired signal(s) may be sent through a subspace without attenuation. The authors of [8] showed that the feasibility of IA is highly dependent on system parameters, such as the numbers of transmitters and receivers, configuration of transmit/receive antennas, etc. IA-based beamforming was proposed in [9] to improve the downlink performance of multiple cell-edge users in multi-user MIMO (Multiple-input multiple-output) systems. A CoMP mechanism incorporated with IA was proposed in [10] for multi-cell multi-user downlink systems based on partial information exchange where both IA and successive decoding are employed. Although this method can improve system throughput, it requires the user-side cooperation which is impractical due to the limited capability of, and the overhead at mobile terminals, non-interoperability between different operators, etc. The authors of [11] proved that the DoFs with CoMP transmission using a two-stage scheme involving both zero forcing and IA can be significantly greater than without CoMP transmission. In [12], by leveraging the locality of interference a distributed interference alignment and cancellation scheme were proposed to overcome the limitations of either requiring data and channel state information (CSI) sharing for all links or having limited capability of interference suppression in the existing CoMP system.

For wireless networks, interference can be not only aligned but also canceled or partially canceled through multiple paths, which is referred to as *interference neutralization* (IN) [13]–[18]. IN seeks to properly combine signals arriving from various paths in such a way that the interfering signals are canceled while the desired signals are preserved [13]. It can be regarded as a distributed zero forcing of interference [14], i.e., transmissions from separate sources cancel each other at a destination without either source actually forming a null to the destination. Note that in practical communications, the interfering transmitters may have their own transmission demands, i.e., the data from multiple transmitters are always different. So, how to incorporate data transmission with interference elimination is a critical issue in the IN-based mechanism design. The authors of [13] constructed a linear distributed IN scheme that encodes in both space and time for separated multiuser uplink-downlink two-way communications. In [14], an aligned IN was proposed in a multi-hop interference network formed by concatenation of two two-user interference channels. The mechanism provides a way to align interference terms over each hop in a manner that allows them to be canceled over the air at the last hop. In [15], the use of IN in a general multi-hop network was studied and a set of feasibility constraints for a subset of links to be active simultaneously was developed. The authors of [16] investigated the feasibility of IN in partially connected relay-aided MIMO interference broadcast channel and discussed the necessary and sufficient condition for IN feasibility using linear transceiver and the achievable DoFs region. In [17], [18], instantaneous relay (relay-without-delay) was introduced to achieve a higher capacity than conventional relays. With those schemes, relays receive desired and interference signals from source nodes and reconstruct them before forwarding to the destinations so as to achieve partial interference elimination (i.e., IN) at the destinations and preserve the desired signal. Although the studies based on instantaneous relay can provide some useful theoretical results, this type of relay is too idealistic. In addition, most of the existing work [13]–[18] investigated IN in multi-hop interference relay channels. By exploiting the broadcast feature of wireless communications, relay nodes receive both desired and interference signals, then apply proper signal reconstruction to implement IN at the destination. However, dedicated relay nodes are needed, which may increase the system cost and complexity. Moreover, in some practical cases, relays may not be necessary.

From the above discussion, one can see that IA and IN have different features and application requirements, to be specific, IA is an interfering-transmitter-based method consuming DoF(s) at the victim receiver whereas IN is a non-interfering-transmitter-based strategy which costs transmit power for generating the neutralizing signal [19]. To the best of our knowledge, most existing works either study IA [10]–[12] individually in CoMP transmission or investigate IN [13]–[18] in relay networks. Although the authors in [20] studied the DoFs of the MIMO multipair two-way distributed relay channel and established a general framework for the DoF analysis by combining the ideas of IA and IN, the application of IN therein still relies on the use of relay nodes. That is, the results provided in the abovementioned works cannot be applied to CoMP with various system settings. Thus, comprehensive use of IA and IN in CoMP is of great research significance. Motivated by the above observations, we exploit the cooperative capability of eNBs (or eNodeBs) in LTE system to propose a CoMP mechanism incorporating both IA and IN (IAN-CoMP) [21]. With IAN-CoMP, data symbols are properly assigned to collaborating eNBs, and precoding and filtering algorithms are jointly designed, so that concurrent transmissions of multiple data streams is achieved.

Moreover, the authors of [22] studied the DoF of the $K-$user interference channel with CoMP transmission and reception which is referred to as the *CoMP channel*. Their system involves K transmitter-receiver pairs with each transmitter having a message wanted by the respective receiver. By introducing two parameters capturing the level of cooperation at the transmitter and the receiver side, i.e., transmit cooperation order M_t and receive cooperation order M_r, the DoF of CoMP channel has been analyzed in depth, yielding some useful results. Inspired by [22], we find that our CoMP model is *non-uniform* whereas the one used in [22] is *uniform*. We then perform a DoF analysis in the non-uniform case.

The contributions of this paper are three-fold:

- Based on the different features and requirements of IA and IN, a CoMP transmission scheme employing interference alignment and neutralization is proposed so as to exploit the advantages of IA in cooperation overhead and IN in DoF cost, respectively. Both IA and IN are

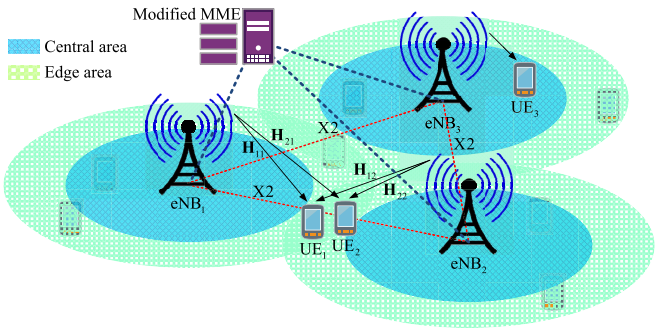

Fig. 1. System model.

adopted for appropriately adjusting interfering signals carrying different and identical information, respectively, so that effective interference cancellation and suppression, as well as multiple concurrent data transmissions can be achieved.

- The proposed scheme is extended to general cases where the numbers of antennas at both transmitter and receiver, the numbers of eNBs participating in CoMP and simultaneously served UEs are variable. Both single-location and multi-location-based implementations of IAN-CoMP are discussed. Moreover, our scheme could make a flexible tradeoff between cooperation overhead and achievable DoFs.
- A DoF analysis in a non-uniform CoMP model is presented. By defining the average cooperation order at the transmitter and receiver sides, respectively, the non-uniform model subsumes the uniform one as a special case. Then, some results derived from the uniform CoMP channel [22] are applied to the non-uniform case.

In this paper, the terminology DoF is defined as the number of concurrent interference-free data streams the system can support. Throughout this paper, we use the following notations. The set of complex numbers is denoted by $\mathbb{C}$, while vectors and matrices are represented by bold lower-case and upper-case letters, respectively. Let $\mathbf{X}^H$, $\mathbf{X}^{-1}$, $\mathbf{X}^\dagger$, $\mathbf{X}^T$ and $\det(\mathbf{X})$ denote the Hermitian, inverse, Moore-Penrose pseudoinverse, transpose, and determinant of matrix $\mathbf{X}$. $\|\cdot\|$ indicates the Euclidean norm. $E(\cdot)$ denotes statistical expectation. $\langle \mathbf{a}, \mathbf{b} \rangle$ represents the inner product of two vectors.

II. System Model

Let's consider a CoMP system [21] consisting of a cluster of adjacent cells as shown in Fig. 1. Downlink transmission is studied. We use M and L to denote the numbers of eNBs and UEs, respectively. The number of antennas at each base station, i.e., eNB_i $(i = 1, 2, \ldots, M)$ is N_T. The eNBs operate in a synchronized slot structure. In each time slot, eNB allocates different resource block to its UEs, so that CCI within a cell is avoided. UEs are randomly distributed in the network. For clarity, only three UEs are clearly plotted of which two are located in the overlapping area of two cells whereas the other one lies in the central area of a cell. The unclear UEs in Fig. 1 indicate those are not scheduled in the current slot. The number of antennas at each UE_j $(j = 1, 2, \ldots, L)$ is N_R. We assume that UE_1 is affiliated with eNB_1 whereas eNB_2 and eNB_3 are the home BSs for UE_2 and UE_3, respectively. For cell-edge users, they would suffer CCI from adjacent eNBs. As for the central area UEs, they will be directly served by their home eNBs without interference. In this paper, we focus on the design of downlink cooperative transmission aiming to improve edge users' communication performance. For clarity of exposition, we begin our design in a specific case in which two eNBs and two UEs, each of them is equipped with two antennas ($N_T = N_R = 2$), are included. Then, in Section IV the proposed scheme is extended to generalized situations.

TABLE I
Major Parameters

Symbol	Definition
M	The number of eNBs
L	The number of UEs
N_T	The number of antennas at each eNB
N_R	The number of antennas at each UE
$\mathbf{H}_{ji}$	Channel matrix between eNB_i and UE_j
P_T	The transmit power at each eNB
$\mathbf{x}_j$	The desired data of UE_j
N_j	The number of UE_j's desired signals
$x_j^{(m)}$	The m^{th} data stream to UE_j
$\omega_j^{(m)}$	The spatial feature of signal carrying $x_j^{(m)}$
$\mathbf{p}_{ji}^{(m)}$	The precoding vector for $x_j^{(m)}$ at eNB_i
$\mathbf{F}_j$	The filter matrix of UE_j
δ_j^{max}	The maximum number of streams UE_j can receive
n_{ji}	The number of streams in $\mathbf{x}_j$ exclusively sent by eNB_i
n_j	The number of streams in $\mathbf{x}_j$ shared over multiple eNBs
Δ	The number of streams served simultaneously to all UEs
$\bar{M}_t$	Average transmit cooperation order
$\bar{M}_r$	Average receive cooperation order

No cooperation is available between UEs [2]. Let $\mathbf{H}_{ji} \in \mathbb{C}^{N_R \times N_T}$ be the channel matrix from eNB_i to UE_j. A spatially uncorrelated Rayleigh flat fading channel model is assumed so that the elements of $\mathbf{H}_{ji}$ are modeled as independent and identically distributed zero-mean unit-variance complex Gaussian random variables. All users experience block fading, i.e., channel parameters in a block consisting of several successive transmission cycles remain constant in the block and vary randomly between blocks. The eNBs can acquire CSI accurately via users' feedback, and share users' data or/and CSI with other eNBs via X2 interface or a modified MME (Mobility management entity). We assume the backhaul dedicated to CSI, data information, and signaling delivery are reliable, with which the latency could be reduced to low, even negligible levels relative to the time scale on which the channel state varies [23], [24]. The transmit power of each eNB, denoted by P_T, is equally distributed over the eNB's transmitted data streams.

The major parameters to be used in this paper are listed in Table I.

III. IAN-Based CoMP Transmission

In this section, we detail an IAN-based CoMP mechanism under specific system settings where $M = 2$, $L = 2$,

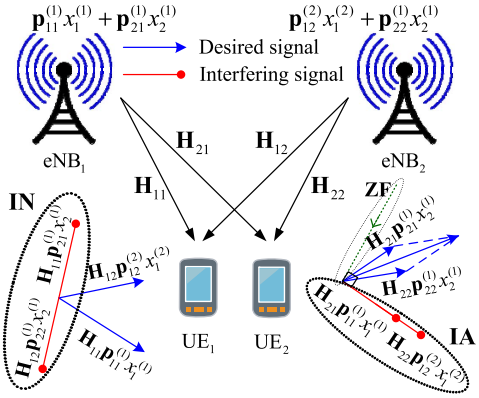

Fig. 2. IAN-CoMP under 2-eNB and 2-UE system settings.

and $N_T = N_R = 2$, with which 3 data streams can be simultaneously supported. We assume that UE_1 is assigned to 2 streams, denoted by $x_1^{(1)}$ and $x_1^{(2)}$, respectively, while UE_2 is served with a single data stream $x_2^{(1)}$. Due to the symmetrical feature of the system model, if UE_1 is served by one stream and UE_2 by two, the proposed scheme is directly applicable. Although the method based on interference alignment and cancellation (IAC) [25] can also achieve the same number of concurrent data streams with an identical system configuration, it requires receiver-side collaboration which is impractical to downlink communications. Moreover, the proposed IAN-based strategy only needs partial users' data sharing between eNBs. Specifically, eNB_1 *transfers* an arbitrary data stream to be sent to UE_1, say $x_1^{(2)}$ to eNB_2, whereas for the data intended for UE_2, i.e., $x_2^{(1)}$, it is *shared* between eNB_2 and eNB_1, then both eNBs transmit $x_2^{(1)}$ to UE_2 cooperatively. According to the above description, each eNB precodes and transmits two data streams to two UEs, as shown in Fig. 2. On one hand, IN is used to adjust two interfering signals of the same data and strength in opposite directions in a subspace such that they can be neutralized at a target UE. On the other hand, IA is applied to align interference signals carrying different information in the same direction in a subspace to reduce the received signal dimension. Based on the cooperative preprocessing at eNBs, ZF is employed at each UE to cancel the residual interference and recover the desired data.

A. IAN-Based Transmit Precoding Design

The mixed signal received at UE_1 and UE_2 can be expressed, respectively, as Eqs. (1) and (2) below:

$$\begin{aligned}\mathbf{y}_1 &= \mathbf{H}_{11}\mathbf{p}_{11}^{(1)}x_1^{(1)} + \mathbf{H}_{12}\mathbf{p}_{12}^{(2)}x_1^{(2)} \\ &\quad + \left(\mathbf{H}_{11}\mathbf{p}_{21}^{(1)} + \mathbf{H}_{12}\mathbf{p}_{22}^{(1)}\right)x_2^{(1)} + \mathbf{z}_1 \qquad (1)\\ \mathbf{y}_2 &= \left(\mathbf{H}_{21}\mathbf{p}_{21}^{(1)} + \mathbf{H}_{22}\mathbf{p}_{22}^{(1)}\right)x_2^{(1)} \\ &\quad + \mathbf{H}_{21}\mathbf{p}_{11}^{(1)}x_1^{(1)} + \mathbf{H}_{22}\mathbf{p}_{12}^{(2)}x_1^{(2)} + \mathbf{z}_2 \qquad (2)\end{aligned}$$

where $\mathbf{H}_{ji} \in \mathbb{C}^{2\times 2}$ $(i,j = 1,2)$. The transmit symbols to UE_1 and UE_2 are denoted by $x_1^{(m)}$ $(m = 1,2)$ and $x_2^{(1)}$, respectively. Here we use the terminologies *data symbol* and *data stream* to mean the same since the latter can be regarded as a continuous process of symbol transmission. Moreover, the analysis in this paper is based on a discrete-time process where the time index is omitted for simplicity. $\mathbf{p}_{ji}^{(m)} \in \mathbb{C}^{N_T\times 1}$ is the precoding vector that eNB_i adopts for data $x_j^{(m)}$ to transmit to UE_j.

The first two terms on the right hand side (RHS) of Eq. (1) indicate the expected signal for UE_1, whereas the third term denotes the interference caused by the transmission of shared data $x_2^{(1)}$ from two collaborating eNBs to UE_2. The first term on the RHS of Eq. (2) represents the expected transmission to UE_2, whereas the second and third terms denote the interference caused by the transmission of $x_1^{(1)}$ from eNB_1 to UE_1 and $x_1^{(2)}$ from eNB_2 to UE_1, respectively. $\mathbf{z}_j \in \mathbb{C}^{N_R\times 1}$ is an additive white Gaussian noise (AWGN) vector whose elements have zero-mean and variance σ_n^2. $E(\mathbf{z}_j\mathbf{z}_j^H) = \sigma_n^2\mathbf{I}_{N_R}$, where $\mathbf{I}_{N_R}$ is an $N_R \times N_R$ identity matrix. Based on the above description, both eNBs send $x_2^{(1)}$ to UE_2, i.e., $x_2^{(1)}$ is *shared* by two eNBs. As for UE_1, its intended data $x_1^{(1)}$ and $x_1^{(2)}$ are precoded and transmitted by two eNBs, respectively, i.e., one data is *transferred* from eNB_1 to eNB_2. Therefore, $E(\|x_1^{(m)}\|^2) = P_T/2$ $(m = 1,2)$, $E(\|x_2^{(1)}\|^2) = P_T/2$.

From Eq. (1), one can see that two interfering signals carry same data $x_2^{(1)}$, so that joint precoding can be designed to achieve IN at UE_1. As for (2), there are two different interferences carrying $x_1^{(1)}$ and $x_1^{(2)}$, respectively. Hence, IA is employed to align the interferences in one direction at UE_2. Then, UE_2 can implement ZF to cancel the aligned interference and recover its expected information (see Section III-B for details). It should be noted that the direction in which two interferences align at UE_2 may be optimized to enhance transmission performance. Due to limited space, we only investigate the alignment based on the subspace determined by $\mathbf{H}_{21}\mathbf{p}_{11}^{(1)}$ or $\mathbf{H}_{22}\mathbf{p}_{12}^{(2)}$.

The precoding vectors designed for eNB should therefore meet the following conditions:

$$\begin{cases}\mathbf{H}_{11}\mathbf{p}_{21}^{(1)} + \mathbf{H}_{12}\mathbf{p}_{22}^{(1)} = \mathbf{0} \\ \mathbf{H}_{21}\mathbf{p}_{11}^{(1)} = \mathbf{H}_{22}\mathbf{p}_{12}^{(2)}\end{cases} \qquad (3)$$

We can then obtain:

$$\begin{cases}\mathbf{p}_{22}^{(1)} = -\mathbf{H}_{12}^{-1}\mathbf{H}_{11}\mathbf{p}_{21}^{(1)} \\ \mathbf{p}_{12}^{(2)} = \mathbf{H}_{22}^{-1}\mathbf{H}_{21}\mathbf{p}_{11}^{(1)}\end{cases} \qquad (4)$$

The second equation in Eq. (4) is to design $\mathbf{p}_{12}^{(2)}$ such that $\mathbf{H}_{22}\mathbf{p}_{12}^{(2)}$ aligns in the direction determined by $\mathbf{H}_{21}\mathbf{p}_{11}^{(1)}$. Similarly, we can also design $\mathbf{p}_{11}^{(1)} = \mathbf{H}_{21}^{-1}\mathbf{H}_{22}\mathbf{p}_{12}^{(2)}$ so as to make $\mathbf{H}_{21}\mathbf{p}_{11}^{(1)}$ align in the subspace determined by $\mathbf{H}_{22}\mathbf{p}_{12}^{(2)}$. For a concise analysis, we introduce equivalent matrices $\mathbf{G}_1 = \mathbf{H}_{22}^{-1}\mathbf{H}_{21}$ and $\mathbf{G}_2 = \mathbf{H}_{12}^{-1}\mathbf{H}_{11}$. Then a general form of precoder, $\mathbf{p}_{j2}^{(m)} = (-1)^m\mathbf{G}_j\mathbf{p}_{j1}^{(1)}$ where $(m,j) \in \{(1,2),(2,1)\}$, is obtained. Note that when antenna configurations are generalized (see Section IV-A for detail), the inverse of channel matrix should be replaced by Moore-Penrose pseudo-inverse so as to calculate the precoders.

From the above general expression we can see that in order to calculate $\mathbf{p}_{j2}^{(m)}$, $\mathbf{p}_{j1}^{(1)}$ should be determined first. Applying the singular value decomposition (SVD) to $\mathbf{H}_{j1}$ $(j = 1,2)$, we get $\mathbf{H}_{j1} = \mathbf{U}_{j1}\mathbf{D}_{j1}\mathbf{V}_{j1}^H$ where $\mathbf{U}_{j1} = [\mathbf{u}_{j1}^{(1)}\ \mathbf{u}_{j1}^{(2)}]$,

$\mathbf{D}_{j1} = \begin{bmatrix} \lambda_{j1}^{(1)} & 0 \\ 0 & \lambda_{j1}^{(2)} \end{bmatrix}$ and $\mathbf{V}_{j1} = [\mathbf{v}_{j1}^{(1)} \ \mathbf{v}_{j1}^{(2)}]$. The column vectors of $\mathbf{U}_{j1}$ and $\mathbf{V}_{j1}$ indicate spatial features, whereas non-zero principal diagonal elements of $\mathbf{D}_{j1}$, sorted in descending order, represent for the amplitude gains of a set of decoupled parallel subchannels. In order to achieve as high a transmission rate as possible, we adopt $\mathbf{p}_{j1}^{(1)} = \mathbf{v}_{j1}^{(1)}$, i.e., the principal subchannel with the maximum singular value $\lambda_{j1}^{(1)}$ is selected. Then, Eqs. (1) and (2) can be rewritten as (5) and (6) below:

$$\mathbf{y}_1 = \lambda_{11}^{(1)}\mathbf{u}_{11}^{(1)}x_1^{(1)} + \mathbf{H}_{12}\mathbf{G}_1\mathbf{v}_{11}^{(1)}x_1^{(2)} + \mathbf{z}_1 \quad (5)$$

$$\mathbf{y}_2 = \left(\lambda_{21}^{(1)}\mathbf{u}_{21}^{(1)} - \mathbf{H}_{22}\mathbf{G}_2\mathbf{v}_{21}^{(1)}\right)x_2^{(1)} + \mathbf{H}_{21}\mathbf{v}_{11}^{(1)}\left(x_1^{(1)} + x_1^{(2)}\right) + \mathbf{z}_2 \quad (6)$$

Here we should note that although $\mathbf{p}_{j1}^{(1)}$ is a unit vector, $\mathbf{p}_{j2}^{(1)}$ is probably not. Moreover, in order to achieve IN, the two signals should have the same strength and be with opposite direction; whereas for IA, only identical direction is required. As a consequence, $\mathbf{p}_{12}^{(2)}$ should be normalized before using so that neither power gain nor attenuation is introduced. However, $\mathbf{p}_{22}^{(1)}$ cannot be scaled due to the purpose of IN. In practice, we can adjust the signal with a higher channel gain to neutralize the one with a lower gain so as to avoid additional power cost. For example, when $\|\mathbf{H}_{11}\mathbf{p}_{21}^{(1)}\| > \|\mathbf{H}_{12}\mathbf{p}_{22}^{(1)}\|$, a coefficient $\zeta_{21}^{(1)} = \|\mathbf{H}_{12}\mathbf{p}_{22}^{(1)}\|/\|\mathbf{H}_{11}\mathbf{p}_{21}^{(1)}\|$ will be introduced so as to achieve $\zeta_{21}^{(1)}\|\mathbf{H}_{11}\mathbf{p}_{21}^{(1)}\| = \|\mathbf{H}_{12}\mathbf{p}_{22}^{(1)}\|$.

From Eq. (5) one can see that the interferences caused by the transmission of $x_2^{(1)}$ from eNB_1 and eNB_2 to UE_2 are neutralized at UE_1 via IN. Eq. (6) indicates that the interferences caused by sending $x_1^{(1)}$ and $x_1^{(2)}$ from two eNBs to UE_1 align in the same direction at UE_2 with IA. However, the interference is not eliminated, as shown in (6). Next, we elaborate the design of receive filter to cancel the residual interference and recover the expected information.

B. Design of Receive Filter

In this subsection, ZF is employed to cancel the residual interference and decode the expected data. Note that no user-side collaboration is assumed, so each UE implements post-processing independently.

Adopt $\mathbf{F}_j^H = [\mathbf{f}_j^{(1)} \ \mathbf{f}_j^{(2)}]^H$ to denote the filter matrix of $\mathbf{y}_j$ where $j = 1, 2$. For simplicity, let $\mathbf{C}_1^{(1)} = \lambda_{11}^{(1)}\mathbf{u}_{11}^{(1)} = \|\mathbf{C}_1^{(1)}\|\mathbf{u}_{\mathbf{C}_1^{(1)}}$, $\mathbf{C}_1^{(2)} = \mathbf{H}_{12}\mathbf{G}_1\mathbf{v}_{11}^{(1)} = \|\mathbf{C}_1^{(2)}\|\mathbf{u}_{\mathbf{C}_1^{(2)}}$, $\mathbf{C}_2^{(1)} = \lambda_{21}^{(1)}\mathbf{u}_{21}^{(1)} - \mathbf{H}_{22}\mathbf{G}_2\mathbf{v}_{21}^{(1)} = \|\mathbf{C}_2^{(1)}\|\mathbf{u}_{\mathbf{C}_2^{(1)}}$ and $\mathbf{C}_2^{(2)} = \mathbf{H}_{21}\mathbf{v}_{11}^{(1)} = \|\mathbf{C}_2^{(2)}\|\mathbf{u}_{\mathbf{C}_2^{(2)}}$. The amplitude of $\mathbf{C}_j^{(m)}$ is $\|\mathbf{C}_j^{(m)}\|$ whereas $\mathbf{u}_{\mathbf{C}_j^{(m)}} = \mathbf{C}_j^{(m)}/\|\mathbf{C}_j^{(m)}\|$ indicates the direction of $\mathbf{C}_j^{(m)}$. These coefficients are substituted into (5) and (6) and $\mathbf{F}_j^H$ is adopted as the filter to obtain Eqs. (7) and (8).

$$\bar{\mathbf{y}}_1 = \mathbf{F}_1^H\|\mathbf{C}_1^{(1)}\|\mathbf{u}_{\mathbf{C}_1^{(1)}}x_1^{(1)} + \mathbf{F}_1^H\|\mathbf{C}_1^{(2)}\|\mathbf{u}_{\mathbf{C}_1^{(2)}}x_1^{(2)} + \mathbf{F}_1^H\mathbf{z}_1 \quad (7)$$

$$\bar{\mathbf{y}}_2 = \mathbf{F}_2^H\|\mathbf{C}_2^{(1)}\|\mathbf{u}_{\mathbf{C}_2^{(1)}}x_2^{(1)} + \mathbf{F}_2^H\|\mathbf{C}_2^{(2)}\|\mathbf{u}_{\mathbf{C}_2^{(2)}}\left(x_1^{(1)} + x_1^{(2)}\right) + \mathbf{F}_2^H\mathbf{z}_2 \quad (8)$$

Note that $\mathbf{C}_2^{(2)}$ is essentially the coefficient of interference part of the mixed signal received by UE_2. The design of receive filter should meet the following condition:

$$\left(\mathbf{f}_j^{(m)}\right)^H\mathbf{u}_{\mathbf{C}_j^{(m')}} = \begin{cases} \alpha_j^{(m)}, & m = m' \\ 0, & m \neq m' \end{cases} \quad (9)$$

where $m, m', j = 1, 2$ and $1 \geq \|\alpha_j^{(m)}\| > 0$. Then, the receive filter for UE_j is calculated as:

$$\mathbf{f}_j^{(m)} = \frac{\mathbf{u}_{\mathbf{C}_j^{(m)}} - \mathbf{u}_{\mathbf{C}_j^{(m')}}^H\mathbf{u}_{\mathbf{C}_j^{(m)}}\mathbf{u}_{\mathbf{C}_j^{(m')}}}{\left\|\mathbf{u}_{\mathbf{C}_j^{(m)}} - \mathbf{u}_{\mathbf{C}_j^{(m')}}^H\mathbf{u}_{\mathbf{C}_j^{(m)}}\mathbf{u}_{\mathbf{C}_j^{(m')}}\right\|}, \quad m \neq m' \quad (10)$$

Substituting (10) into (7) and (8), we get (11) and (12), shown at the bottom of this page. According to (11), the desired data $x_1^{(1)}$ and $x_1^{(2)}$ of UE_1 can be decoded, respectively, in two mutually orthogonal subspaces. As for (12), the expected data $x_2^{(1)}$ of UE_2 is recovered in the subspace orthogonal to the one in which residual interference, indicated by the second term on the RHS of (12), is located.

C. Achievable Spectral-Efficiency Analysis

By observing the noise parts in (11) and (12), although co-channel interference is eliminated and the expected data is decoded in an interference-free subspace, $\mathbf{F}_j$ is not a unitary matrix, i.e., $\langle\mathbf{f}_j^{(1)}, \mathbf{f}_j^{(2)}\rangle \neq 0$. As a result, the noise power after receive filtering becomes:

$$E\left\{(\mathbf{F}_j^H\mathbf{z}_j)(\mathbf{F}_j^H\mathbf{z}_j)^H\right\} = E\left\{\mathbf{F}_j^H\mathbf{z}_j\mathbf{z}_j^H\mathbf{F}_j\right\} = \sigma_n^2\mathbf{A}_j \quad (13)$$

where

$$\mathbf{A}_j = \begin{bmatrix} 1 & (\mathbf{f}_j^{(1)})^H\mathbf{f}_j^{(2)} \\ (\mathbf{f}_j^{(2)})^H\mathbf{f}_j^{(1)} & 1 \end{bmatrix}.$$

Given $E(\|x_1^{(m)}\|^2) = P_T/2$ where $m = 1, 2$ and $E(\|x_2^{(1)}\|^2) = P_T/2$, The achievable spectral efficiency for each UE is computed as Eqs. (14) and (15), shown at the bottom of the next page. The effect of $\mathbf{A}_j$ on R_1 and R_2 has been studied in [26]. For space limitations we do not discuss it in this paper.

$$\bar{\mathbf{y}}_1 = \left\|\mathbf{C}_1^{(1)}\right\|\begin{bmatrix} (\mathbf{f}_1^{(1)})^H\mathbf{u}_{\mathbf{C}_1^{(1)}} \\ 0 \end{bmatrix}x_1^{(1)} + \left\|\mathbf{C}_1^{(2)}\right\|\begin{bmatrix} 0 \\ (\mathbf{f}_1^{(2)})^H\mathbf{u}_{\mathbf{C}_1^{(2)}} \end{bmatrix}x_1^{(2)} + \mathbf{F}_1^H\mathbf{z}_1 \quad (11)$$

$$\bar{\mathbf{y}}_2 = \left\|\mathbf{C}_2^{(1)}\right\|\begin{bmatrix} (\mathbf{f}_2^{(1)})^H\mathbf{u}_{\mathbf{C}_2^{(1)}} \\ 0 \end{bmatrix}x_2^{(1)} + \left\|\mathbf{C}_2^{(2)}\right\|\begin{bmatrix} 0 \\ (\mathbf{f}_2^{(2)})^H\mathbf{u}_{\mathbf{C}_2^{(2)}} \end{bmatrix}\left(x_1^{(1)} + x_1^{(2)}\right) + \mathbf{F}_2^H\mathbf{z}_2 \quad (12)$$

IV. Generalization of IAN-CoMP

In this section, we extend IAN-CoMP to general cases while varying antenna configurations at both the transmitter and receiver sides, the numbers of eNBs participating in CoMP and simultaneously served UEs. Before delving into details, we first provide one theorem and three corollaries on IA and IN.

Theorem 1: Each of the signals generated to achieve interference alignment or neutralization at an unintended receiver while being decoded at their intended receiver should be originated from a different transmitter.

Proof sketch: Take the transmission of $x_1^{(1)}$ and $x_1^{(2)}$ as an example, as shown in Fig. 2. If both are sent from eNB$_i$ and aligned in one direction at their unintended receiver UE$_2$, where $i \in \{1, \cdots, M\}$ is the index of eNB, then $\mathbf{H}_{2i}\mathbf{p}_{2i}^{(1)} = \mathbf{H}_{2i}\mathbf{p}_{2i}^{(2)}$. One can easily see that these two signals also overlap with each other at their intended receiver UE$_1$, thus becoming indistinguishable. As for IN, if the signal carrying $x_1^{(1)}$ is neutralized at UE$_2$, then $\mathbf{H}_{2i}\mathbf{p}_{2i}^{(1)}x_1^{(1)} = -\mathbf{H}_{2i}\mathbf{p}_{2i'}^{(1)}x_1^{(1)}$, where $\mathbf{p}_{2i'}^{(1)}$ represents the precoder for a duplicate signal to mitigate the original interference $\mathbf{H}_{2i}\mathbf{p}_{2i}^{(1)}x_1^{(1)}$ at UE$_2$. Then, the two signals will also be neutralized at any other UE$_j$ where user index $j \in \{1, \cdots, L\}$ and $j \neq 2$. ■

Corollary 1: If $\kappa > 1$ interferences are from an identical transmitter, they should be mapped into a κ-dimensional space at their unintended receivers so as to be distinguishable at their intended receiver(s).

Proof sketch: According to Theorem 1, if Corollary 1 is not satisfied, at least two signal components will overlap with each other at a UE, thus becoming indistinguishable. Thus, Corollary 1 follows. ■

Corollary 2: The same set of signals cannot be simultaneously aligned with each other at more than one receiver.

Proof sketch: Take the transmission of $x_1^{(1)}$ and $x_1^{(2)}$ as an example. According to Theorem 1, they should be sent by two eNBs, say eNB$_1$ and eNB$_2$, separately, so as to be aligned in one direction at a UE. Without loss of generality, if two signals carrying $x_1^{(1)}$ and $x_1^{(2)}$ are aligned with each other at UE$_1$ and UE$_2$, then $\mathbf{H}_{1i}\mathbf{p}_{1i}^{(1)} = \mathbf{H}_{1i'}\mathbf{p}_{1i'}^{(2)}$ and $\mathbf{H}_{2i}\mathbf{p}_{1i}^{(1)} = \mathbf{H}_{2i'}\mathbf{p}_{1i'}^{(2)}$ where $i, i' \in \{1, 2\}$ and $i \neq i'$, should be satisfied simultaneously. Due to the randomness of channel conditions, given $\mathbf{p}_{1i}^{(1)}$ (or $\mathbf{p}_{1i'}^{(2)}$), a solution for the other precoder $\mathbf{p}_{1i'}^{(2)}$ (or $\mathbf{p}_{1i}^{(1)}$), satisfying both equations, usually does not exist. ■

Similar to Corollary 2, we can derive the following corollary.

Corollary 3: The same pair of signals cannot be neutralized at more than one receiver simultaneously.

Proof sketch: The proof is similar to that in Corollary 2. ■

In what follows, we extend the proposed IAN-CoMP to more general cases.

A. Generalized Antenna Configurations

The proposed IAN-CoMP can be extended to the general situation in which the antenna configurations at both transmitter and receiver sides are variable. Since mobile stations/devices are subject to severer restrictions such as cost and hardware than a base station, we assume $N_T \geq N_R$. For clarity, our discussion is confined to 2-eNB 2-UE system settings.

Let $\mathbf{x}_1 = [x_1^{(1)} \ \cdots \ x_1^{(N_R)}]^T$ and $\mathbf{x}_2 = [x_2^{(1)} \ \cdots \ x_2^{(N_R-1)}]^T$ denote the desired data of UE$_1$ and UE$_2$, respectively. Vectors $\mathbf{x}_{11} = [x_1^{(1)} \ \cdots \ x_1^{(N_R-1)}]^T$ and $\mathbf{x}_2$ are sent by eNB$_1$, whereas $\mathbf{x}_{12} = [x_1^{(1)} \ \cdots \ x_1^{(N_R-2)} \ x_1^{(N_R)}]^T$ and $\mathbf{x}_2$ are sent by eNB$_2$. In other words, UE$_1$'s data, except $x_1^{(N_R-1)}$ and $x_1^{(N_R)}$, is *shared* over both eNBs. eNB$_1$ *transfers* $x_1^{(N_R)}$ to eNB$_2$ whereas $x_1^{(N_R-1)}$ is sent by eNB$_1$ exclusively. In addition, both eNBs transmit $\mathbf{x}_2$ to UE$_2$ cooperatively. In the above description, $x_1^{(N_R-1)}$ and $x_1^{(N_R)}$ are taken as an example in the mechanism design. In practice, any two arbitrary data streams, say $x_1^{(m)}$ and $x_1^{(n)}$ $(m \neq n)$, can be used. Our scheme is still applicable in such cases. For simplicity, an equal power allocation is adopted, i.e., $E(\|x_1^{(m)}\|^2) = E(\|x_2^{(n)}\|^2) = P_T/(2N_R-2)$ where $m = 1, \cdots, N_R$ and $n = 1, \cdots, N_R-1$.

Given the above system configurations, the received mixed signal at UE$_1$ and UE$_2$ can be expressed as (16) and (17), shown at the bottom of this page, where $\mathbf{H}_{ji} \in \mathbb{C}^{N_R \times N_T}$ $(i, j = 1, 2)$. $\mathbf{p}_{1i}^{(m)} \in \mathbb{C}^{N_T \times 1}$ $(m = 1, \cdots, N_R)$ is the precoding vector for data $x_1^{(m)}$ that eNB$_i$ transmits to UE$_1$. $\mathbf{P}_i^{(\mathbf{x}_2)} \in \mathbb{C}^{N_T \times (N_R-1)}$ represents the precoding matrix for $\mathbf{x}_2$ that eNB$_i$ transmits to UE$_2$. The first three terms on the RHS

$$R_1 = \sum_{m=1}^{2} R_1^{(m)} = \sum_{m=1}^{2} \log_2 \left\{ \det \left[\mathbf{I}_{N_R} + \frac{P_T \left(\mathbf{F}_1^H \mathbf{C}_1^{(m)}\right)\left(\mathbf{F}_1^H \mathbf{C}_1^{(m)}\right)^H}{2\sigma_n^2 \mathbf{A}_1} \right] \right\} \tag{14}$$

$$R_2 = \log_2 \left\{ \det \left[\mathbf{I}_{N_R} + \frac{P_T \left(\mathbf{F}_2^H \mathbf{C}_2^{(1)}\right)\left(\mathbf{F}_2^H \mathbf{C}_2^{(1)}\right)^H}{2\sigma_n^2 \mathbf{A}_2} \right] \right\} \tag{15}$$

$$\mathbf{y}_1 = \sum_{m=1}^{N_R-2} \left[\mathbf{H}_{11}\mathbf{p}_{11}^{(m)} + \mathbf{H}_{12}\mathbf{p}_{12}^{(m)}\right] x_1^{(m)} + \mathbf{H}_{11}\mathbf{p}_{11}^{(N_R-1)}x_1^{(N_R-1)} + \mathbf{H}_{12}\mathbf{p}_{12}^{(N_R)}x_1^{(N_R)} + \left[\mathbf{H}_{11}\mathbf{P}_1^{(\mathbf{x}_2)} + \mathbf{H}_{12}\mathbf{P}_2^{(\mathbf{x}_2)}\right]\mathbf{x}_2 + \mathbf{z}_1 \tag{16}$$

$$\mathbf{y}_2 = \left[\mathbf{H}_{21}\mathbf{P}_1^{(\mathbf{x}_2)} + \mathbf{H}_{22}\mathbf{P}_2^{(\mathbf{x}_2)}\right]\mathbf{x}_2 + \sum_{m=1}^{N_R-2} \left[\mathbf{H}_{21}\mathbf{p}_{11}^{(m)} + \mathbf{H}_{22}\mathbf{p}_{12}^{(m)}\right] x_1^{(m)} + \mathbf{H}_{21}\mathbf{p}_{11}^{(N_R-1)}x_1^{(N_R-1)} + \mathbf{H}_{22}\mathbf{p}_{12}^{(N_R)}x_1^{(N_R)} + \mathbf{z}_2 \tag{17}$$

TABLE II
THE ACHIEVABLE DOFS OF EACH UE UNDER VARIOUS DATA-EXCHANGE CONDITIONS

Index	δ_1^{max}	δ_2^{max}	n_{11}	n_{12}	n_2
1	N_R	N_R-1	1	1	N_R-1
2	N_R	N_R-n_{11}	$n_{11}\geq 1$	1	N_R-n_{11}
3	N_R	N_R-n_{11}	$n_{11}\geq 1$	0	N_R-n_{11}
4	N_R	N_R-n_{12}	1	$n_{12}\geq 1$	N_R-n_{12}
5	N_R	N_R-n_{12}	0	$n_{12}\geq 1$	N_R-n_{12}
6	N_R	$N_R-\max(1,n_{11},n_{12})$	n_{11}	n_{12}	$N_R-\max(1,n_{11},n_{12})$
7	N_R-1	N_R-1	1	1	N_R-2
8	$\max(1,n_{11},n_{12})+n_2$	$N_R-\max(1,n_{11},n_{12})$	n_{11}	n_{12}	n_2

of (16) indicate the desired signal for UE_1, whereas the fourth term denotes the interference caused by the transmission of shared data $\mathbf{x}_2$ from two cooperating eNBs to UE_2. In (17), the first term on the RHS represents the expected transmission to UE_2, whereas the next three terms denote the interference caused by the transmission of $\mathbf{x}_{11}$ from eNB_1 to UE_1 and $\mathbf{x}_{12}$ from eNB_2 to UE_1, respectively. In (16), two interference signals carry the same data $\mathbf{x}_2$, and hence joint precoding can be adopted to achieve IN at UE_1. In (17), IA is employed to align the interferences in one direction so that the mixed signal's dimension is reduced at UE_2. The precoding vectors designed for eNB should thus meet the following conditions:

$$\begin{cases}\mathbf{H}_{11}\mathbf{P}_1^{(\mathbf{x}_2)}+\mathbf{H}_{12}\mathbf{P}_2^{(\mathbf{x}_2)}=\mathbf{0}\\ \mathbf{H}_{21}\mathbf{p}_{11}^{(m)}+\mathbf{H}_{22}\mathbf{p}_{12}^{(m)}=\mathbf{H}_{21}\mathbf{p}_{11}^{(N_R-1)}=\mathbf{H}_{22}\mathbf{p}_{12}^{(N_R)}\end{cases} \quad (18)$$

According to Theorem 1, in the second equation of (18), since $\mathbf{H}_{21}\mathbf{p}_{11}^{(N_R-1)}=\mathbf{H}_{22}\mathbf{p}_{12}^{(N_R)}$ holds, the solutions for $\mathbf{p}_{11}^{(m)}$ and $\mathbf{p}_{12}^{(m)}$ w.r.t. $\mathbf{H}_{21}\mathbf{p}_{11}^{(m)}=\mathbf{H}_{21}\mathbf{p}_{11}^{(N_R-1)}$ and $\mathbf{H}_{22}\mathbf{p}_{12}^{(m)}=\mathbf{H}_{22}\mathbf{p}_{12}^{(N_R)}$ alone are not available. In order to solve this problem, we let both eNBs transmit $x_1^{(m)}$ $(m=1,\cdots,N_R-2)$ and align the combined signal $\mathbf{H}_{21}\mathbf{p}_{11}^{(m)}+\mathbf{H}_{22}\mathbf{p}_{12}^{(m)}$ with either $\mathbf{H}_{21}\mathbf{p}_{11}^{(N_R-1)}$ or $\mathbf{H}_{22}\mathbf{p}_{12}^{(N_R)}$, so that all interferences at UE_2 are aligned in one direction. However, according to the second sub-equation in Eq. (18), to achieve IA in this cooperative way, we can guarantee either $\|\mathbf{p}_{11}^{(m)}\|=1$ or $\|\mathbf{p}_{12}^{(m)}\|=1$.

Similarly to the design in previous section, all precoders can be calculated. Thus, the interferences caused by the transmission of $\mathbf{x}_2$ from two eNBs to UE_2 are neutralized at UE_1, and the interferences caused by the transmission of $\mathbf{x}_{11}$ and $\mathbf{x}_{12}$ from two eNBs to UE_1 are aligned in the same direction at UE_2. ZF is then adopted to cancel the residual interference and recover the desired information. Due to space limitation, we omit design details at the receiver side which can be found in Section III. The total achievable DoFs of the given system is thus $2N_R-1$ with the extended IAN-CoMP of which N_R data streams are for UE_1 and the other N_R-1 streams for UE_2.

The system model for $M=2$, $L=2$, and $N_T=N_R=2$ can be characterized by a MIMO X channel [27] whose achievable DoFs have been studied extensively. Researchers have also proposed various schemes to obtain such DoFs, in which techniques including zero-forcing, IA [28], successive decoding and dirty paper coding (DPC) [29] are employed. However, to the best of our knowledge, IN has not been considered. The achievable DoFs for a MIMO X channel where each node is equipped with N antennas increase according to $4N/3$ for no shared messages $\rightarrow$ $3N/2$ for partial information shared from one transmitter to the other which is feasible for downlink $\rightarrow$ $2N$ for full cooperation between transmitters, i.e., broadcast channels [27]. The proposed IAN-CoMP could achieve as high as $2N_R-1$ DoFs with partial cooperation under $N_T\geq N_R$ and 2-eNB 2-UE system settings, but the overhead w.r.t. data sharing and transferring between two eNBs is high. Fortunately, we can make a flexible tradeoff between cooperation cost and achievable system DoFs. Let δ_1^{max}, δ_2^{max}, n_{11}, n_{12} and n_2 denote, respectively, the maximum number of data streams UE_1 and UE_2 can receive, the number of streams in $\mathbf{x}_1$ exclusively sent by eNB_1 and eNB_2, and the number of data symbols in $\mathbf{x}_2$ *shared* over both eNBs. Table II shows the achievable DoFs of each UE under various data-exchange conditions.

From cases 1 to 3, one can see that given $n_{11}\geq 1$, $n_{11}\geq n_{12}$ and all data streams intended for UE_2 are shared over two eNBs, i.e., $\delta_2^{max}=n_2$, δ_1^{max} can be as large as N_R. This is because that interfering signals cooperatively sent by two eNBs counteract with each other at UE_1. As for UE_2, based on Eq. (18) and Corollary 1, an $n_{11}-$dimensional space is required at UE_2 for accommodating n_{11} interferences from eNB_1. So, the achievable DoFs of UE_2 is $\delta_2^{max}=N_R-n_{11}$. When $n_{12}\geq 1$ and $n_{12}\geq n_{11}$, as shown by cases 4 and 5 in Table II, δ_1^{max} and δ_2^{max} are N_R and N_R-n_{12}, respectively. The analysis is similar to that of the previous three cases. In case 6, the impacts of n_{11} and n_{12} on δ_1^{max} and δ_2^{max} are taken into account. Since the use of IA consumes at least one DoF at UE_2, we get $\delta_2^{max}=N_R-\max(1,n_{11},n_{12})$. Case 7 shows the influence of n_2 on δ_1^{max} and δ_2^{max}. Due to the application of IA, $\delta_2^{max}=N_R-1$. As for UE_1, n_2 data streams in $\mathbf{x}_2$ are shared and cooperatively sent by both eNBs to achieve IN at UE_1. Thus, the remaining $\delta_2^{max}-n_2$ streams intended for UE_2 will result in the same DoF cost at UE_1, yielding $\delta_1^{max}=N_R-(\delta_2^{max}-n_2)$. The last row shows general expressions of δ_1^{max} and δ_2^{max}. The achievable DoFs of the system can be easily obtained as $\delta_1^{max}+\delta_2^{max}$.

From the above discussion, we can see that to achieve the maximum system DoFs, i.e., N_R+n_2, a total number of $\max(1,n_{11},n_{12})-n_{11}-n_{12}+2n_2$ data streams should be shared over, or transferred between the two eNBs. Taking the design in Section III as an example where $n_{11}=n_{12}=1$ and $n_2=N_R-1$, with $2N_R-3$ data-exchange overhead, UE_1 and UE_2 can receive N_R and N_R-1 independent streams, respectively.

B. Generalized Number of eNBs

We now generalize the number of eNBs, denoted by M, participating in CoMP. The number of UEs, L, is fixed at 2. We first present two properties of applying IA and IN in a multi-eNB multi-UE downlink system as depicted in Fig. 2.

Property 1: When IA is applied once, (say) K signals are aligned in one direction at one of their unintended receivers. These interferences can be mitigated at the cost of 1 DoF, but at each of the other unintended receivers, K DoFs will be consumed.

Property 2: When IN is applied once, one interference signal can be mitigated at one of its unintended receivers without consuming any DoF, but 1 DoF is consumed at each of the other unintended receivers.

Based on Property 2, for L receivers, one-time use of IN will consume a total of $L-2$ DoFs. Here two users are exempted from L, one of which is the intended, and the other is the undesired receiver where IN is implemented.

Using the above two properties, we can define the *cost-effectiveness ratio of interference management*, η, as the total number of DoFs consumed by IM at all receivers divided by the number of interference signals that can be mitigated. Then, we can get:

$$\begin{cases} \eta_{IA} = \left[1 + (L-2)K_{IA}\right]/K_{IA} = L - 2 + K_{IA}^{-1} \\ \eta_{IN} = (L-2)K_{IN}/K_{IN} = L-2 \end{cases} \tag{19}$$

where K_{IA} and K_{IN} are the numbers of aligned and neutralized signals, respectively.

Note that L should be at least 2 for multi-user CoMP transmission. When $L=2$, K interferences could be mitigated at the expense of 1 DoF, so $\eta_{IA} = 1/K_{IA}$. As for IN, one interference could be eliminated at no cost of DoFs, thus $\eta_{IN} = 0$. Eq. (19) shows that as L grows larger than 2, both η_{IA} and η_{IN} are greater than 1 and increase accordingly, i.e., more DoFs are consumed for interference mitigation.

In practice, IA and IN can be realized at a single location — i.e., all signal components are aligned in one direction or paired and neutralized at a single UE — or at multiple locations — i.e., various subsets of interferences are aligned and neutralized at multiple UEs. Without loss of generality, we will first discuss a single-location-based implementation in the following extension of IAN-CoMP, and then present the extension with a multi-location-based realization in Section IV-D.

Suppose $M > 2$, $L = 2$ and $N_R \geq M$, i.e., UE has sufficient antennas to decode its information. Similarly to the processing shown in Fig. 2, IN is implemented at UE_1 while IA is achieved at UE_2. The difference between $M=2$ (Section III) and $M>2$ lies in the fact that when $M=2$, there are only two signal components of $\mathbf{x}_1$ which are sent by eNB_1 and eNB_2, respectively; for the other signals intended to UE_1, they are cooperatively sent by both eNBs so as to achieve alignment at UE_2. In case of $M>2$, at most M signals could be explicitly sent by the eNBs whereas for the remainders, cooperative transmissions could be done by C_M^2 combinations of eNB-pairs. Since signals intended for UE_2, i.e., $\mathbf{x}_2$, are neutralized at UE_1, we have $\delta_1^{max} = N_R$. As for UE_2, using IA consumes 1 DoF, hence $\delta_2^{max} = N_R - 1$.

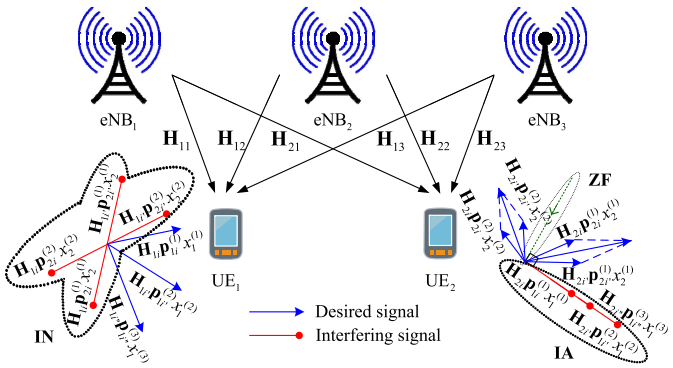

Fig. 3. IAN-CoMP extension under 3-eNB and 2-UE system settings.

So, when $M > 2$ eNBs participate in CoMP, we can achieve a selection diversity gain from multiple eNBs while keeping the total system DoFs intact. Taking system settings $M=3$, $L=2$, $N_R=3$, and $N_T \geq N_R$ as an example, the proposed IAN-CoMP can be implemented as shown in Fig. 3. The extension of IAN-CoMP to more general M can be readily achieved.

In Fig. 3, the subscripts i, i' and i'' indicate the indices of eNBs, and $i \neq i' \neq i''$. As can be seen in this instance, $x_1^{(1)}$, $x_1^{(2)}$ and $x_1^{(3)}$ are sent by three eNBs, respectively, so that IA is achieved at UE_2. Moreover, $x_2^{(1)}$ and $x_2^{(2)}$ are sent from two arbitrarily selected eNB-pairs, and two corresponding signal-pairs achieve IN at UE_1 separately. As a result, we support a total of five concurrent streams, three of which are intended for UE_1 and two for UE_2.

C. Generalized Number of UEs

Here we generalize the number of simultaneously served UEs, $L > 2$. For simplicity of presentation, the number of eNBs, M is fixed at 2, and $N_R \geq M$.

We assume IN is implemented at UE_1, and IA is achieved at UE_2, i.e., single-location-based implementation is considered. According to Corollaries 2 and 3, signals achieving IN or IA at one UE cannot establish the same relationship at the other UEs. Also, based on Eq. (18), signals intended to UE_1 can be explicitly or cooperatively sent by the two eNBs so as to achieve IA at UE_2. In addition, since more CCI is introduced as L increases, the achievable DoFs of a user are dependent on those of the others. So, we get $\delta_1^{max} = N_R - (L-1)$, $\delta_2^{max} = N_R - 1 - \sum_{l=3}^{L} \delta_l^{max}$ and $\delta_j^{max} = N_R - \sum_{l=1, l\neq j}^{L} \delta_l^{max}$ $(j = 3, \ldots, L)$ where l and j are the indices of UEs. By observing the expression of δ_j^{max} $(j \geq 3)$ and observing that $\delta_j^{max} \geq 1$ $(j = 1, \cdots, L)$, we have:

$$\begin{cases} \sum_{l=1}^{L} \delta_l^{max} = N_R \\ \sum_{l=3}^{L} \delta_l^{max} \leq N_R - 2 \\ \sum_{l=1, l\neq j}^{L} \delta_l^{max} \leq N_R - 1, \quad j = 3, \cdots, L \\ \delta_j^{max} > 0, \qquad\qquad\qquad j = 1, \cdots, L \end{cases} \tag{20}$$

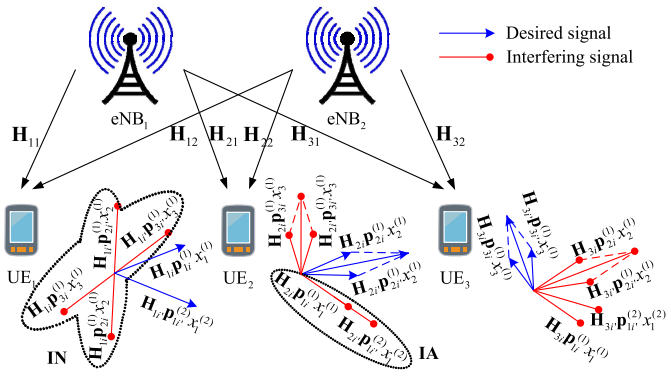

Fig. 4. Multi-location-based implementation of IAN-CoMP. (a) $M \geq 2$, $L = 3$, $N_R = 4$. (b) $M \geq 2$, $L = 3$, $N_R = 5$.

From the first equation in (20) we can see that when $L > 2$, the achievable system DoFs are N_R. Moreover, since $\delta_1^{max} \geq 1$, we get $L \leq N_R$. Therefore, at most $L = N_R$ users can be simultaneously supported, each being served by a single data stream.

Taking the system settings $M = 2$, $L = 3$, $N_R = 4$, and $N_T \geq N_R$ as an example, with a single-location-based implementation, $(\delta_1^{max}, \delta_2^{max}, \delta_3^{max})$ can be selected from the set $\{(2,1,1),\ (1,2,1),\ (1,1,2)\}$ so that 4 independent data streams can be simultaneously supported. So, there could be various ways to allocate DoFs to multiple users. In practice, round-robin [30], weighted fair scheduling [31], and other channel allocation algorithms can be employed for DoFs distribution. Due to space limitation, we do not elaborate them in this paper.

Fig. 4 shows the extension of IAN-CoMP under $(\delta_1^{max}, \delta_2^{max}, \delta_3^{max}) = (2,1,1)$. As can be seen, $x_1^{(1)}$ and $x_1^{(2)}$ are explicitly sent, whereas $x_2^{(1)}$ and $x_3^{(1)}$ are cooperatively sent by the two eNBs, so that IA and IN are achieved at UE_2 and UE_1, respectively. Given the other $(\delta_1^{max}, \delta_2^{max}, \delta_3^{max})$ values, the proposed IAN-CoMP can be implemented similarly at a single UE.

D. Multi-Location-Based Implementation of IAN-CoMP

As for the multi-location-based case, since interference subsets for alignment and neutralization as well as the number of data streams allocated to each user can vary, the realization of IAN-CoMP becomes more flexible than that of the single-location-based case.

We use K_{IA} and K_{IN} to denote the numbers of aligned and neutralized signals, respectively. For simplicity, we assume only one IM method, i.e., IA or IN, is realized at a UE in the following discussion. As can be seen from Eq. (19), given K signals and L UEs, applying IN can save one more DoF compared to using IA. Thus, although IA can be realized at multiple UEs, i.e., dividing K_{IA} signals into multiple disjoint subsets and applying IA to signals in each subset separately, due to its higher DoF cost compared to IN, the single-location-based implementation of IA at only one UE, incurring 1 DoF cost, is preferable. One should also notice that although IN has advantage over IA in terms of DoF cost, IN requires more collaboration between eNBs. Moreover, IN incurs extra power cost when generating a neutralizing signal compared to conventional IA [19], whereas for the cooperative realization of IA, additional power is also consumed.

By noticing that the transmission of one data stream consumes 1 DoF at its intended receiver and the total available DoFs at the receiver side is LN_R. Then Eq. (21) should hold,

$$K_{IN}\left[1 + (L-2)\right] + \left[K_{IA} + 1 + (L-2)K_{IA}\right] = LN_R \tag{21}$$

When applying IN to a signal, 1 DoF is used for the desired transmission to its intended receiver, no DoF is consumed at the UE where IN is realized, and 1 DoF is occupied by the interfering signal at each of the remaining $L-2$ UEs. As for IA, K_{IA} signals use K_{IA} DoFs at their desired UE(s), 1 DoF is consumed at the UE where IA is implemented, and K_{IA} DoFs are occupied by the interferences at each of the remaining $L-2$ UEs.

Since the use of IA takes either 1 or K_{IA} DoFs at any unintended UE, K_{IN} is limited to $N_R - 1$. Then the achievable system DoF can be calculated according to:

$$\begin{aligned} &\text{maximize}(K_{IA} + K_{IN}) \\ &s.t.\ K_{IN} \leq N_R - 1 \\ &\quad K_{IA} = \left\lfloor \frac{N_R L - 1}{L-1} - K_{IN} \right\rfloor \end{aligned} \tag{22}$$

where $\lfloor \cdot \rfloor$ indicates rounding down to the nearest integer. The expression of K_{IA} can be derived from Eq. (21). When $\frac{N_R L-1}{L-1}$ is an integer, $K_{IN} = N_R - 1$ and $K_{IA} = \frac{N_R+L-2}{L-1}$ could achieve $K_{IN} + K_{IA} = \frac{N_R L-1}{L-1}$ DoFs, being equal to the achievable system DoF. In this case, IA should be realized at a single UE; otherwise, such a system DoF cannot be achieved. When $\frac{N_R L-1}{L-1}$ is a fractional number, IA could be implemented at either a single UE or multiple UEs so as to achieve the maximum system DoFs, i.e., $\lfloor \frac{N_R L-1}{L-1} \rfloor$, which can be realized by adopting $K_{IN} = N_R - 1$ and $K_{IA} = \lfloor \frac{N_R+L-2}{L-1} \rfloor$. Note that there are various combinations of K_{IA} and K_{IN} that can output the maximum system DoFs. The above discussion only shows an example.

In Fig. 5 we take the system settings $M \geq 2$, $L = 3$, $N_R = 4$ and $M \geq 2$, $L = 3$, $N_R = 5$ as examples to illustrate various implementations of multi-location IAN-CoMP. Given other system settings, the proposed scheme can be similarly realized. For the clarity of exposition, we do not show the eNBs and UEs. As shown in Fig. 5(a), the maximum system DoF is 5. Since $\frac{N_R L-1}{L-1} = \frac{11}{2}$ is a fractional, although IA is realized at two UEs separately in the first subcase, incurring more DoF cost, the maximum system DoF can still be achieved. In the second subcase, $K_{IA} + K_{IN} = 3 + 2 = 5$, IN is implemented at two UEs whereas IA is realized at only one UE. Although 1 DoF is left unused at UE_2, neither IA nor IN can make use of it due to the DoF limitation at the other UEs. In Fig. 5(b), $\frac{N_R L-1}{L-1} = 7$ is an integer, thus multi-location-based implementation of IA cannot achieve the maximum system DoF. As can be seen in the first subcase of subfigure (b), only 6 concurrent transmissions are supported, whereas in the second subcase, IA is realized only at one UE,

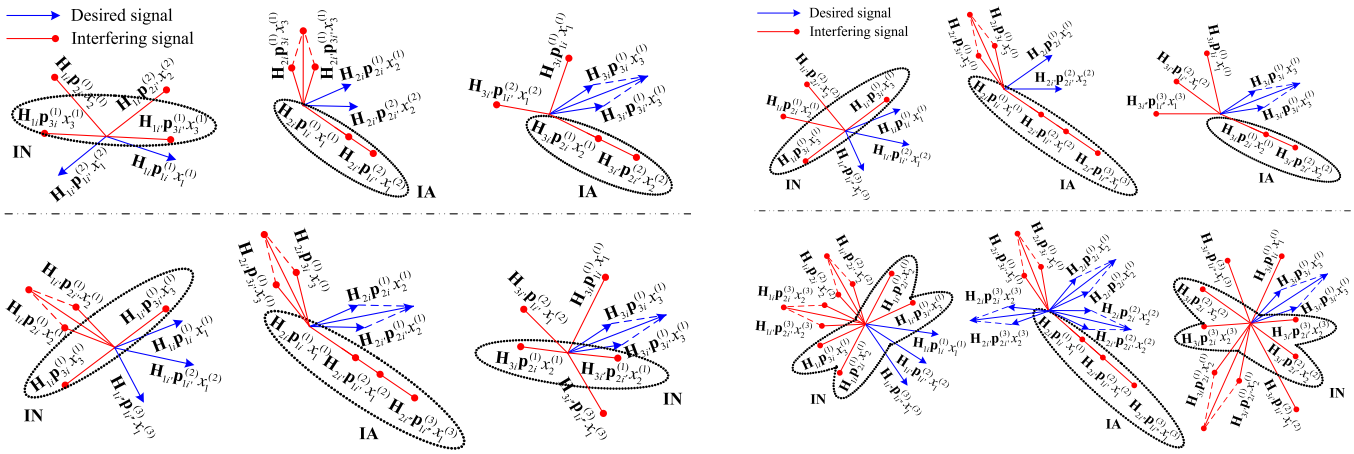

(a) $M \geq 2$, $L = 3$, $N_R = 4$. (b) $M \geq 2$, $L = 3$, $N_R = 5$.

Fig. 5. IAN-CoMP extension under 2-eNB and 3-UE system settings.

TABLE III
COMPARISON OF ACHIEVABLE DOFS WITH TWO IAN-COMP IMPLEMENTATIONS

Parameter settings	Single-location IAN-CoMP	Multi-location IAN-CoMP
$L = 3$, $N_R = 3$	3	4
$L = 3$, $N_R = 4$	4	5
$L = 3$, $N_R = 5$	5	7
$L = 4$, $N_R = 5$	5	6

then the maximum system DoF, $K_{IA} + K_{IN} = 3 + 4 = 7$, is produced.

We now use Table III to compare the DoF performance of the two IAN-CoMP implementations under $N_T \geq N_R$, $L > 2$ and $M > 2$ as below.

From Table III one can see that multi-location IAN-CoMP outperforms the single-location-based realization in achievable system DoFs. Given $L > 2$, since $\left\lfloor \frac{N_R-1}{L-1} \right\rfloor > 0$ can be derived from $\left\lfloor \frac{N_R L-1}{L-1} \right\rfloor > N_R$, that is, when inequality $\left\lfloor \frac{N_R-1}{L-1} \right\rfloor > 0$ holds, the number of achievable DoFs with multi-location IAN-CoMP exceeds that with single-location IAN-CoMP. Since N_R and L are always greater than 1 in practice, as long as $N_R > L$, $\left\lfloor \frac{N_R-1}{L-1} \right\rfloor > 0$ holds, and thus multi-location IAN-CoMP can provide more DoFs than the single-location one. When $L = 2$, according to the assumption that only one IM method is realized at a UE, multi-location IAN-CoMP becomes single-location IAN-CoMP. However, if we discard this restriction, multi-location IAN-CoMP can be realized by letting $N_R - 1$ data streams of UE_2 be neutralized at UE_1, while UE_1's κ ($\kappa = 2, \cdots, N_R - 1$) data streams be aligned at UE_2 and UE_1's remaining $N_R - \kappa$ streams be neutralized at UE_2, respectively. Therefore, $2N_R - 1$ DoFs can be achieved; this is identical to that with the single-location IAN-CoMP. Based on the above analysis, multi-location IAN-CoMP can subsume single-location IAN-CoMP as a special case, thus is more general.

E. Generalized Description of the IAN-CoMP

Based on the above discussion, we now give a generalized description of the proposed IAN-CoMP in this subsection. Although the following presentation is with respect to the single-location-based implementation, as for the multi-location-based realization, only the UEs at which IA and IN are realized are varied while signal processing is similar to that in the single-location-based scheme.

The eNBs acquire CSI via their UEs' feedback and inter-eNB collaboration. The desired data of UE_j ($j = 1, \cdots, L$) is $\mathbf{x}_j = [x_j^{(1)} \; x_j^{(2)} \; \cdots \; x_j^{(N_j)}]$. We use N_j to denote the number of desired signals for UE_j. $N_1 \leq N_R$, $N_2 \leq N_R - 1$, $\sum_{j=3}^{L} N_j \leq N_R - 2$ and $\sum_{j=1}^{L} N_j = N_R$ should hold. With the single-location-based implementation, IN and IA are exclusively implemented at UE_1 and UE_2, respectively.

At UE_1, in order to exploit IN to cancel the unintended signals, we let the transmission of an interfering data stream, say $x_j^{(m)}$ ($j \neq 1$) be carried out by eNB_i and $\text{eNB}_{i'}$ cooperatively. So that precoders for $x_j^{(m)}$ should satisfy $\mathbf{H}_{1i}\mathbf{p}_{ji}^{(m)} + \mathbf{H}_{1i'}\mathbf{p}_{ji'}^{(m)} = \mathbf{0}$. Then according to Eqs. (3) and (4) we can get $\mathbf{p}_{ji'}^{(m)} = -\mathbf{H}_{1i'}^{-1}\mathbf{H}_{1i}\mathbf{p}_{ji}^{(m)}$, where $\mathbf{p}_{ji}^{(m)}$ can be obtained by applying SVD to $\mathbf{H}_{ji}$.

At UE_2, IA is employed to align the signals intended to UE_1 in one direction. Two situations are considered as follows,

- When $M \geq N_1$, N_1 out of M eNBs can be selected to form a set $\mathcal{A}$, each eNB in the set exclusively sends one desired data stream to UE_1 satisfying $\mathbf{H}_{2i}\mathbf{p}_{1i}^{(m)} = \mathbf{H}_{2i_{ref}}\mathbf{p}_{1i_{ref}}^{(m_{ref})}$ where $m, m_{ref} \in \{1, \cdots, N_1\}$, $\text{eNB}_i, \text{eNB}_{i_{ref}} \in \mathcal{A}$ and $|\mathcal{A}| = N_1$. $\mathbf{H}_{2i_{ref}}\mathbf{p}_{1i_{ref}}^{(m_{ref})}$ represents the referential spatial feature of a data stream which can be selected arbitrarily from those intended to UE_1. All the other UE_1's desired signals should be aligned with such a referential direction.

Then we can get $\mathbf{p}_{1i}^{(m)} = \mathbf{H}_{2i}^{-1}\mathbf{H}_{2i_{ref}}\mathbf{p}_{1i_{ref}}^{(m_{ref})}$ where $\mathbf{p}_{1i_{ref}}^{(m_{ref})}$ can be obtained via the SVD of $\mathbf{H}_{1i_{ref}}$.

- When $M < N_1$, only M data streams intended to UE$_1$ can be exclusively sent by the M eNBs whereas for the remaining $N_1 - M$ streams, each of them should be shared over and cooperatively sent from two eNBs. So that equation $\mathbf{H}_{2\tilde{i}}\mathbf{p}_{1\tilde{i}}^{(\tilde{m})} + \mathbf{H}_{2\tilde{i}'}\mathbf{p}_{1\tilde{i}'}^{(\tilde{m})} = \mathbf{H}_{2i}\mathbf{p}_{1i}^{(m)} = \mathbf{H}_{2i_{ref}}\mathbf{p}_{1i_{ref}}^{(m_{ref})}$ should hold, where $\tilde{m}$ is the index of a data stream cooperatively sent by eNB$_{\tilde{i}}$ and eNB$_{\tilde{i}'}$. The alignment of the signals exclusively sent by an eNB is the same with that in the $M \geq N_1$ case. Based on the above analysis, we can have $\mathbf{p}_{1\tilde{i}'}^{(\tilde{m})} = \mathbf{H}_{2\tilde{i}'}^{-1}[\mathbf{H}_{2i_{ref}}\mathbf{p}_{1i_{ref}}^{(m_{ref})} - \mathbf{H}_{2\tilde{i}}\mathbf{p}_{1\tilde{i}}^{(\tilde{m})}]$. Similarly to the previous discussion, $\mathbf{p}_{1i_{ref}}^{(m_{ref})}$ and $\mathbf{p}_{1\tilde{i}}^{(\tilde{m})}$ can be acquired by applying SVD to $\mathbf{H}_{1i_{ref}}$ and $\mathbf{H}_{1\tilde{i}}$, respectively.

Note that the above analysis is done under the assumption of $N_T = N_R$. When $N_T > N_R$, the inverse of channel matrix should be replaced by Moore-Penrose pseudo-inverse.

As for the design of receive filter at UE$_j$ where $j \in \{1, \cdots, L\}$, in order to decode $x_j^{(m)}$ ($m \in \{1, \cdots, N_j\}$), the filter vector for the m^{th} data stream to UE$_j$, denoted by $\mathbf{f}_j^{(m)}$, should satisfy:

$$\left(\mathbf{f}_j^{(m)}\right)^H \omega_{j'}^{(m')} = \begin{cases} \alpha_j^{(m)}, & j' = j \text{ and } m' = m \\ 0, & j' \neq j \text{ or } m' \neq m \end{cases} \quad (23)$$

where $j' \in \{1, \cdots, L\}$, $m' \in \{1, \cdots, N_{j'}\}$ and $|\alpha_j^{(m)}| \in (0, 1)$. $\omega_{j'}^{(m')}$ represents the spatial feature of the signal carrying $x_{j'}^{(m')}$. There are two situations should be taken into account.

- When $x_{j'}^{(m')}$ is exclusively sent from an eNB, $\omega_{j'}^{(m')} = \mathbf{H}_{ji}\mathbf{p}_{j'i}^{(m')}/\|\mathbf{H}_{ji}\mathbf{p}_{j'i}^{(m')}\|$.
- When $x_{j'}^{(m')}$ is sent from two eNBs, say eNB$_i$ and eNB$_{i'}$, cooperatively, $\omega_{j'}^{(m')} = (\mathbf{H}_{ji}\mathbf{p}_{j'i}^{(m')} + \mathbf{H}_{ji'}\mathbf{p}_{j'i'}^{(m')})/\|\mathbf{H}_{ji}\mathbf{p}_{j'i}^{(m')} + \mathbf{H}_{ji'}\mathbf{p}_{j'i'}^{(m')}\|$.

To design $\mathbf{f}_j^{(m)}$, we first construct a matrix $\mathbf{\Pi}_j^{(m)} \in \mathbb{C}^{N_R \times (N_R - 1)}$ consisting of the spatial features of all the interfering components w.r.t. $x_j^{(m)}$'s transmission perceived by UE$_j$. Next, by applying Gram-Schmidt orthogonalization to $\mathbf{\Pi}_j^{(m)}$, a set of orthonormal basis, say $\widetilde{\mathbf{\Pi}}_j^{(m)}$ consisting of $\tilde{\omega}_{j'}^{(m')}$ where $j' \neq j$ or $m' \neq m$, is obtained. Then, we project $\omega_j^{(m)}$, the spatial feature of the signal carrying $x_j^{(m)}$, onto the orthogonal subspace spanned by $\widetilde{\mathbf{\Pi}}_j^{(m)}$ to get an intermediate vector, denoted by $\hat{\mathbf{f}}_j^{(m)}$. Finally, we normalize $\hat{\mathbf{f}}_j^{(m)}$ to get the filter vector $\mathbf{f}_j^{(m)}$. So, the receive filter at UE$_j$, denoted by $\mathbf{F}_j = [\mathbf{f}_j^{(1)}\ \mathbf{f}_j^{(2)}\ \cdots\ \mathbf{f}_j^{(N_j)}]$, can be obtained.

F. Analysis of Upper Bound for IAN-CoMP

The number of DoFs of IAN-CoMP is limited by the CoMP system with certain cooperation capability. In [22], the maximum DoFs of a CoMP channel under various cooperation conditions has been studied in depth. However, the system model employed in [22] is *uniform* whereas our CoMP system is featured as *non-uniform*. First, the numbers of transmit and receive antennas are not necessarily the same in our design, while they are the same in [22]. Second, with IAN-CoMP the cooperation level at the transmitter side is non-uniform. That is, not all messages are shared over, and cooperatively processed by the same number of transmit antennas. Third, limited and non-uniform cooperation is exploited at the receiver side, i.e., only joint processing with multiple antennas of the same UE is considered without inter-UE collaboration. As a result, we cannot use the transmit and receive cooperation order, i.e., M_t and M_r, defined in [22] directly to indicate the cooperation level of our IAN-CoMP. So, in order to utilize the results provided in [22] to analyze the bound of our scheme, we need to extend the assessment of cooperation level from the uniform case to the non-uniform one.

Motivated by the definition of M_t and M_r in [22], we first define *average transmit cooperation order* and *average receive cooperation order* as $\bar{M}_t$ and $\bar{M}_r$, respectively. Note that the cooperation of transmit and receive antennas is related to independent data streams (messages) from the transmitter to the receiver side, and in the non-uniform case, different messages may have different cooperation levels. We take 2-eNB, 2-UE, and $N_T = N_R = 2$ as an example, since $x_1^{(1)}$ and $x_1^{(2)}$ are exclusively sent by eNB$_1$ and eNB$_2$ which are equipped with 2 antennas, the cooperation levels of $x_1^{(1)}$ and $x_1^{(2)}$ are 2, while as $x_2^{(1)}$ is shared over, and sent by eNB$_1$ and eNB$_2$ cooperatively, its cooperation level is 4. Moreover, since there exist two types of transmit cooperation, i.e., cooperation of N_T antennas equipped with a single eNB and $2N_T$ antennas of two cooperative eNBs, we use "I" and "II" to indicate these two cooperation modes/levels. As inter-UE cooperation is assumed unavailable in our work, only one receive cooperation mode, i.e., cooperation of N_R antennas of a single UE exists. We call a set of cooperative antennas for a message's transmission/reception a *cooperation antenna group* (CAG) at the transmitter/receiver side. If a message is jointly processed by a CAG, we say that this CAG is used once; otherwise, if $m > 1$ data streams are cooperatively processed by an identical CAG, the number of times this CAG is used is counted to be m. Thus, the expression of $\bar{M}_t$ is given as:

$$\bar{M}_t = \frac{1}{K_{Ant.,t}K_{Data}} \sum_{\mathcal{M} \in \{I, II\}} m_t^{\mathcal{M}} K_{CAG,t}^{\mathcal{M}} M_t^{\mathcal{M}} \quad (24)$$

where $K_{Ant.,t}$ and K_{Data} represent the numbers of transmit antennas and independent data streams with the IAN-CoMP scheme. Superscript $\mathcal{M} \in \{I, II\}$ denotes the index of cooperation mode. $m_t^{\mathcal{M}}$ and $M_t^{\mathcal{M}}$ are the number of messages and cooperation level of message(s) with cooperation mode $\mathcal{M}$ at the transmitter side. $K_{CAG,t}^{\mathcal{M}}$ is the number of times that CAG(s) with mode $\mathcal{M}$ is used at the transmitter side.

Similarly, $\bar{M}_r$ is defined as:

$$\bar{M}_r = \frac{m_r^I K_{CAG,r}^I M_r^I}{K_{Ant.,r}K_{Data}} \quad (25)$$

where $K_{Ant.,r}$ denotes the number of antennas at the receiver side. Since there is only one cooperation type at the

TABLE IV
COOPERATION PARAMETERS UNDER VARIOUS SYSTEM SETTINGS

System settings				$K_{Ant.,t}$,	K_{Data},	$M_t^{\mathcal{M}}$		$K_{CAG,t}^{\mathcal{M}}$		$m_t^{\mathcal{M}}$		$\bar{M}_t$	M_r^I	$\bar{M}_r$	DoFs	Bound [22]
M	L	N_T	N_R	$K_{Ant.,r}$	$K_{CAG,r}^I$,m_r^I	I	II	I	II	I	II					
2	2	2	2	4	3	2	4	2	1	2	1	1	2	$\frac{3}{2}$	3	3
3	3	3	3	9	4	3	6	2	2	2	2	1	3	$\frac{4}{3}$	4	5
3	3	4	4	12	5	4	8	2	3	2	3	$\frac{22}{15}$	4	$\frac{5}{3}$	5	7
3	3	5	5	15	7	5	10	3	4	3	4	$\frac{41}{22}$	5	$\frac{7}{3}$	7	9
3	4	4	3	12	3	4	8	1	2	1	2	1	3	$\frac{3}{4}$	3	6
5	3	3	5	15	7	3	6	3	4	3	4	$\frac{41}{35}$	5	$\frac{7}{3}$	7	9
M	L	N_T	N_R	$\mathcal{N}$	$\left\lfloor \frac{\mathcal{N}-1}{L-1} \right\rfloor$	N_T	$2N_T$	①	②	①	②	Eq. (28)	N_R	Eq. (29)	$\left\lfloor \frac{\mathcal{N}-1}{L-1} \right\rfloor$	Eq. (30)

① = $\left\lfloor \frac{\mathcal{N}-1}{L-1} \right\rfloor - N_R + 1$, ② = $N_R - 1$

receiver side, we use the fixed superscript I for simplicity. m_r^I and M_r^I are the number of messages and cooperation order of message(s) jointly processed at the receiver side. $K_{CAG,r}^I$ is the number of times that CAG(s) is utilized at the receiver side.

Since the results in [22] are obtained under the condition that both transmitter and receiver sides are equipped with the same number of antennas, we will then study the application of such results in our non-uniform CoMP model such that $MN_T = LN_R = \mathcal{N}$, i.e., the numbers of transmit and receive antennas are identical while the transmit/receive cooperation is non-uniform.

In the uniform case [22], all messages have the same cooperation level at either transmitter or receiver side, denoted as M_t and M_r, respectively, so Eqs. (24) and (25) become

$$\bar{M}_t = \frac{m_t K_{CAG,t} M_t}{K_{Ant.,t} K_{Data}} \tag{26}$$

and

$$\bar{M}_r = \frac{m_r K_{CAG,r} M_r}{K_{Ant.,r} K_{Data}}. \tag{27}$$

Since $K_{Ant.,t} = K_{Ant.,r} = K_{CAG,t} = K_{CAG,r} = \mathcal{N}$ [22] and $m_t = m_r = K_{Data}$, we can get $\bar{M}_t = M_t$ and $\bar{M}_r = M_r$. That is, the definition of average cooperation order subsumes the cooperation order defined in [22] as a special case.

Now, let us use Table IV to illustrate the above-mentioned parameters under various system settings, based on which $\bar{M}_t$, $\bar{M}_r$, and the bound of a CoMP system [22] with cooperation level $\bar{M}_t$ and $\bar{M}_r$ are calculated.

Note that all the system settings in Table IV satisfy $MN_T = LN_R = \mathcal{N}$, i.e., the numbers of antennas at the transmitter and receiver sides are the same. Since each message is jointly decoded at a UE, yielding cooperation of N_R antennas which form a CAG, so that $K_{CAG,r}^I$ equals m_r^I which is identical to K_{Data}, and hence for simplicity, we do not explicitly list $K_{CAG,r}^I$ and m_r^I in Table IV. Provided with $L = 2$, the number of achievable DoFs of IAN-CoMP is $2N_R - 1$ (see Section IV-A). While given $L \geq 3$, since multi-location-based implementation of IAN-CoMP could achieve more DoFs than the single-location IAN-CoMP, only the multi-location IAN-CoMP is included in the table. In the last row of Table IV, we present the general expressions of $\bar{M}_t$ and $\bar{M}_r$ under $L \geq 3$. As rows 3–8 of Table IV show, the DoFs obtained with IAN-CoMP (the 2nd column to the right) is no greater than the bound provided in [22] (the 1st column to the right) given the same system settings.

By substituting related parameters into Eqs. (24) and (25), we can have the general expressions of $\bar{M}_t$ and $\bar{M}_r$ under $L \geq 3$ as:

$$\bar{M}_t = N_T \left\{ \frac{1}{\mathcal{N}} \left\lfloor \frac{\mathcal{N}-1}{L-1} \right\rfloor - \frac{2}{L} + \frac{2}{\mathcal{N}} + \frac{3}{\mathcal{N}} \left(\frac{\mathcal{N}}{L} - 1 \right)^2 \left\lfloor \frac{\mathcal{N}-1}{L-1} \right\rfloor^{-1} \right\} \tag{28}$$

and

$$\bar{M}_r = \frac{1}{L} \left\lfloor \frac{\mathcal{N}-1}{L-1} \right\rfloor. \tag{29}$$

According to the Theorems 2 and 3 in [22], given $\bar{M}_t + \bar{M}_r \leq \mathcal{N}$ (i.e., the total cooperation order is no greater than $\mathcal{N}$) or $\bar{M}_t + \bar{M}_r \geq \mathcal{N} + 1$ (this should be modified to $\bar{M}_t + \bar{M}_r > \mathcal{N}$ since $\bar{M}_t$ and $\bar{M}_r$ are always non-integers in our discussion), the outer bound of a CoMP channel is limited by $\lceil \mathcal{B}^* \rceil = \left\lceil \frac{1}{2} \left(\mathcal{N} + \bar{M}_t + \bar{M}_r - 2 \right) \right\rceil$ or equal to $\mathcal{N}$, respectively. By substituting $\mathcal{N}$, $\bar{M}_t$ and $\bar{M}_r$ where $\bar{M}_t + \bar{M}_r \leq \mathcal{N}$, into $\lceil \mathcal{B}^* \rceil$, we can have the outer bound of a CoMP system with average cooperation level $\bar{M}_t$ and $\bar{M}_r$ (given by the first sub-equation of Eq. (30)). Then, we can get

$$\mathcal{B} = \begin{cases} \lceil \mathcal{B}^* \rceil, & \bar{M}_t + \bar{M}_r \leq \mathcal{N} \\ \mathcal{N}, & \bar{M}_t + \bar{M}_r > \mathcal{N} \end{cases} \tag{30}$$

where $\mathcal{B}^* = N_T \left\{ \frac{1}{2\mathcal{N}} \left\lfloor \frac{\mathcal{N}-1}{L-1} \right\rfloor - \frac{1}{L} + \frac{1}{\mathcal{N}} + \frac{3}{2\mathcal{N}} \left(\frac{\mathcal{N}}{L} - 1 \right)^2 \left\lfloor \frac{\mathcal{N}-1}{L-1} \right\rfloor^{-1} \right\} + \frac{1}{2L} \left\lfloor \frac{\mathcal{N}-1}{L-1} \right\rfloor + \frac{\mathcal{N}-2}{2}$.

As can be seen, given $L = 2$, $\left\lfloor \frac{\mathcal{N}-1}{L-1} \right\rfloor = 2N_R - 1$ holds, so that we can use $\left\lfloor \frac{\mathcal{N}-1}{L-1} \right\rfloor$ to indicate the DoFs achieved by IAN-CoMP under $L \geq 2$. In what follows, we will prove the number of DoFs of IAN-CoMP is upper bounded by $\mathcal{B}$. i.e., $\mathcal{B} \geq \left\lfloor \frac{\mathcal{N}-1}{L-1} \right\rfloor$. Since $\left\lfloor \frac{\mathcal{N}-1}{L-1} \right\rfloor$ is strictly less than $\mathcal{N}$ under $L \geq 2$, $\mathcal{B} \geq \left\lfloor \frac{\mathcal{N}-1}{L-1} \right\rfloor$ under $\bar{M}_t + \bar{M}_r > \mathcal{N}$ is proved. Then, we can verify $\lceil \mathcal{B}^* \rceil \geq \left\lfloor \frac{\mathcal{N}-1}{L-1} \right\rfloor$ under $L \geq 2$ when $\bar{M}_t + \bar{M}_r > \mathcal{N}$ (see Appendix). Therefore, given $L \geq 2$, $\mathcal{B} \geq \left\lfloor \frac{\mathcal{N}-1}{L-1} \right\rfloor$ follows.

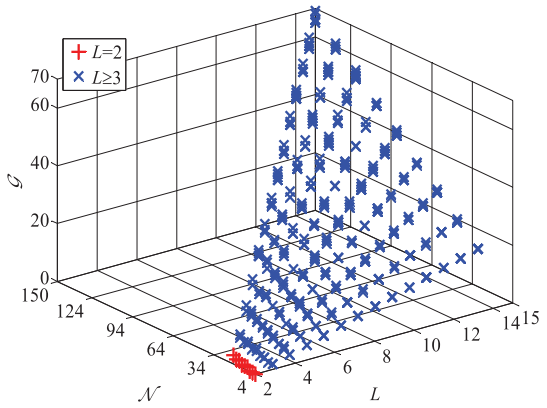

Fig. 6. $\mathcal{G}$ under $MN_T = LN_R = \mathcal{N}$, $N_T \geq N_R$ and $L \geq 2$.

TABLE V
THE COMPLEXITY OF MAIN OPERATIONS

$\mathbf{A}_1 + \mathbf{A}_1$	$2mn$
$\mathbf{A}_1\mathbf{A}_2$	$6mnp + 2mp(n-1)$
$\mathbf{A}_3^{-1}$	$6m^3 + 2m(m-1)^2$
Normalization($\mathbf{A}_1$)	$10mn$
Gram-Schmidt($\mathbf{A}_1$) $(m \geq n)$	$\sim 2mn^2$ [32]
SVD($\mathbf{A}_1$)	$24m^2n + 48mn^2 + 54n^3$ [33]

We also verify $\lceil \mathcal{B}^* \rceil \geq \left\lfloor \frac{\mathcal{N}-1}{L-1} \right\rfloor$ by employing MATLAB simulation. Fig. 6 plots $\mathcal{G} = \lceil \mathcal{B}^* \rceil - \left\lfloor \frac{\mathcal{N}-1}{L-1} \right\rfloor$, under $MN_T = LN_R = \mathcal{N}$, $N_T \geq N_R$ and $L \geq 2$. The number of UEs, L, ranges from 2 to 15. N_R various from 2 to 10.

As the figure shows, the bound $\lceil \mathcal{B}^* \rceil$ is no less than $\left\lfloor \frac{\mathcal{N}-1}{L-1} \right\rfloor$ achieved by the IAN-CoMP proposed in our work. Although only limited number of values of L and N_R are considered in Fig. 6, given other values of L and N_R, $\mathcal{G} \geq 0$ still holds. In practical CoMP system, however, the numbers of cooperative base stations (BSs) and mobile stations (MSs) served by multiple BSs are limited. The simulation results given in Fig. 6 cover possible situations in practical use.

V. ANALYSIS OF COMPUTATIONAL COMPLEXITY

We now analyze the computational complexity of the proposed approach. The complexity is quantified in number of real floating point operations (FLOPs) [32]. A real addition, multiplication, or division is counted as one FLOP. A complex addition and multiplication have two FLOPs and six FLOPs, respectively. For clarity of exposition, we start our analysis from 2-eNB 2-UE system settings with variable N_T and N_R. Without specification, all the following operations are in regard to complex domain calculations. The complexity of main operations related to the proposed IAN-CoMP is given in Table V, where $\mathbf{A}_1 \in \mathbb{C}^{m\times n}$, $\mathbf{A}_2 \in \mathbb{C}^{n\times p}$ and $\mathbf{A}_3 \in \mathbb{C}^{m\times m}$. SVD($\mathbf{A}_1$) and Normalization($\mathbf{A}_1$) indicate applying SVD to and computing the normalization of $\mathbf{A}_1$, respectively. Gram-Schmidt($\mathbf{A}_1$) denotes employing Gram-Schmidt orthogonalization to matrix $\mathbf{A}_1$ so as to obtain its orthonormal basis. The symbol $\sim$ represents for asymptotic value as $m, n \to \infty$ (leading term). In what follows, the computational complexity at transmitter and receiver sides will be detailed, respectively.

Without loss of generality, we adopt $m_{ref} = N_R - 1$, then based on Eq. (18) we can get $\mathbf{P}_2^{(\mathbf{x}_2)} = -\mathbf{H}_{12}^{\dagger}\mathbf{H}_{11}\mathbf{P}_1^{(\mathbf{x}_2)}$, $\mathbf{p}_{12}^{(N_R)} = -\mathbf{H}_{22}^{\dagger}\mathbf{H}_{21}\mathbf{p}_{11}^{(N_R-1)}$ and $\mathbf{p}_{12}^{(m)} = \mathbf{H}_{22}^{\dagger}[\mathbf{H}_{21}\mathbf{p}_{11}^{(N_R-1)} - \mathbf{H}_{21}\mathbf{p}_{11}^{(m)}]$, where $m \in \{1, \cdots, N_R - 2\}$. To calculate the above precoders, we first need to apply SVD to $\mathbf{H}_{11}$ and $\mathbf{H}_{21}$, which takes $2(24N_R^2N_T + 48N_T^2N_R + 54N_T^3)$ FLOPs in total. As for a matrix $\mathbf{H} \in \mathbb{C}^{N_R\times N_T}$, when $N_T > N_R$, according to the Moore-Penrose pseudo-inverse calculation $\mathbf{H}^{\dagger} = \mathbf{H}^H(\mathbf{H}\mathbf{H}^H)^{-1}$, two matrix multiplications and one matrix inversion are needed, so the FLOP count is $16N_R^2N_T + 8N_R^3 - 6N_R^2 - 2N_RN_T + 2N_R$. To obtain $\mathbf{P}_2^{(\mathbf{x}_2)}$, a multiplication of an $N_R \times N_T$ matrix and an $N_T \times (N_R - 1)$ matrix, a multiplication of an $N_T \times N_R$ matrix and an $N_R \times (N_R - 1)$ matrix, and $\mathbf{H}_{12}^{\dagger}$ are required. Then, the FLOP count of $\mathbf{P}_2^{(\mathbf{x}_2)}$ is computed as $32N_R^2N_T + 8N_R^3 - 8N_R^2 - 20N_RN_T + 4N_R + 2N_T$. Similarly, to get $\mathbf{p}_{12}^{(N_R)}$, a multiplication of an $N_R \times N_T$ matrix and an $N_T \times 1$ vector, a multiplication of an $N_T \times N_R$ matrix and an $N_R \times 1$ vector, and the pseudo-inverse of $\mathbf{H}_{22}$ are needed. Moreover, $\mathbf{p}_{12}^{(N_R)}$ should be normalized before use. Thus, the FLOP count of computing $\mathbf{p}_{12}^{(N_R)}$ is $16N_R^2N_T + 8N_R^3 + 14N_RN_T - 6N_R^2 + 8N_T$. As for the calculation of $\mathbf{p}_{12}^{(m)}$, since $\mathbf{H}_{22}^{\dagger}$ and $\mathbf{H}_{21}\mathbf{p}_{11}^{(N_R-1)}$ have been obtained when calculating $\mathbf{p}_{12}^{(N_R)}$, and $\mathbf{H}_{21}\mathbf{p}_{11}^{(m)}$ is of the same complexity with $\mathbf{H}_{21}\mathbf{p}_{11}^{(N_R-1)}$, one addition of two $N_R \times 1$ vectors, one multiplication of an $N_T \times N_R$ matrix and an $N_R \times 1$ vector are needed. So, the FLOP count of computing $\mathbf{p}_{12}^{(m)}$ is $16N_RN_T - 2N_T$. Since $m \in \{1, \ldots, N_R - 2\}$, there are $N_R - 2$ precoders, incurring the total complexity is $16N_R^2N_T - 34N_RN_T + 4N_T$. As a result, the FLOP count of transmitter side processing is $108N_T^3 + 16N_R^3 + 112N_R^2N_T + 96N_RN_T^2 - 14N_R^2 - 40N_RN_T + 4N_R + 14N_T \sim 108N_T^3 + 16N_R^3 + 112N_R^2N_T + 96N_RN_T^2$.

At the receiver side, according to Eq. (16), to decode the desired signal components at UE$_1$, we need to acquire the spatial feature of each signal received by UE$_1$. As indicated by the first term on the RHS of Eq. (16), to get the spatial feature of $x_1^{(m)}$ $(m \in \{1, \cdots, N_R - 2\})$ cooperatively sent by the two eNBs, two multiplications of an $N_R \times N_T$ matrix and an $N_T \times 1$ vector and addition of two $N_R \times 1$ vectors are required, taking $16N_RN_T - 2N_R$ FLOPs. According to the second and third terms on the RHS of Eq. (16), $x_1^{(N_R-1)}$ and $x_1^{(N_R)}$ are sent by an eNB exclusively, and hence calculating each of their spatial features needs one multiplication of an $N_R \times N_T$ matrix and an $N_T \times 1$ vector, which takes $8N_RN_T - 2N_R$ FLOPs. Since the number of signals cooperatively sent by two eNBs and exclusively sent by an eNB are $N_R - 2$ and 2, respectively, the total FLOP count is $16N_R^2N_T - 2N_R^2 - 16N_RN_T \sim 16N_R^2N_T$.

Similarly, to decode the desired signals at UE$_2$, spatial features of the received signal components at UE$_2$ are needed. According to the expression of the first term on the RHS of Eq. (17), $\mathbf{x}_2$, consisting of $N_R - 1$ elements, is sent by both eNBs cooperatively. To compute the spatial feature of each $x_2^{(m)}$ in $\mathbf{x}_2$, $16N_RN_T - 2N_R$ FLOPs are required.

So, its calculation N_R-1 times takes $16N_R^2N_T-2N_R^2-16N_RN_T+2N_R$ FLOPs. As for the second to fourth terms on the RHS of Eq. (17), they are aligned in the same direction, thus only one spatial feature needs to be calculated. Without loss of generality, we take $x_1^{(N_R-1)}$'s feature as an example, which requires $8N_RN_T-2N_R$ FLOPs. So, the total FLOP count for computing the spatial features of all signal components at UE$_2$ is $16N_R^2N_T-2N_R^2-8N_RN_T\sim 16N_R^2N_T$.

To calculate the filter vector $\mathbf{f}_j^{(m)}$ for $x_j^{(m)}$ at UE$_j$ where $j\in\{1,\cdots,L\}$, we first apply Gram-Schmidt orthogonalization to $\mathbf{\Pi}_j^{(m)}\in\mathbb{C}^{N_R\times(N_R-1)}$ so as to obtain its orthonormal basis $\widetilde{\mathbf{\Pi}}_j^{(m)}$, taking $2N_R(N_R-1)^2$ FLOPs. Next, we project $\omega_j^{(m)}$, the spatial feature of signal carrying $x_j^{(m)}$, onto the orthogonal subspace spanned by $\widetilde{\mathbf{\Pi}}_j^{(m)}$, consisting of $\tilde{\omega}_{j'}^{(m')}$ ($j'\in\{1,\cdots,L\}$, $m'\in\{1,\cdots,N_{j'}\}$, $j'\neq j$ or $m'\neq m$), to get an intermediate vector $\hat{\mathbf{f}}_j^{(m)}=\omega_j^{(m)}-\sum_{j'}\sum_{m'}(\tilde{\omega}_{j'}^{(m')})^T\omega_j^{(m)}\tilde{\omega}_{j'}^{(m')}$, which requires N_R-1 multiplications of a $1\times N_R$ vector and an $N_R\times 1$ vector, N_R-1 multiplications of a complex number and an $N_R\times 1$ vector, and N_R-1 additions of two $N_R\times 1$ vectors, taking $16N_R^2-18N_R+2$ FLOPs in total. By normalizing $\hat{\mathbf{f}}_j^{(m)}$, which requires $10N_R$ FLOPs, we then obtain $\mathbf{f}_j^{(m)}$. As a result, to get the receive filter at UE$_j$, $\mathbf{F}_j=[\mathbf{f}_j^{(1)}\ \mathbf{f}_j^{(2)}\ \cdots\ \mathbf{f}_j^{(N_j)}]$, $2N_R^3N_j+12N_R^2N_j-6N_RN_j+2N_j\sim 2N_R^3N_j$ FLOPs are required. The mixed signal perceived by UE$_j$ is then left multiplied by the receive filter $\mathbf{F}_j^H\in\mathbb{C}^{N_j\times N_R}$, which takes N_RN_j multiplications and $(N_R-1)N_j$ additions. The FLOP count is $8N_RN_j-2N_j\sim 8N_RN_j$.

Based on the above analysis, the FLOP count of processing at one UE$_j$ is $\sim 16N_R^2N_T+2N_R^3N_j+8N_RN_j$.

The above analysis is under the assumption of $N_T>N_R$. When $N_T=N_R$, the pseudo-inverse of a matrix should be replaced by its inverse. The Gauss-Jordan elimination can be employed to compute the inverse of an $N_R\times N_R$ matrix, which takes $6N_R^3+2N_R(N_R-1)^2$ FLOPs. As for the remaining computations, they are the same with those in the $N_T>N_R$ situation. So, the FLOP count of the transmitter side processing becomes $108N_T^3+16N_R^3+80N_R^2N_T+96N_RN_T^2-10N_R^2-36N_RN_T+4N_R+14N_T\sim 108N_T^3+16N_R^3+80N_R^2N_T+96N_RN_T^2$, whereas the complexity at a UE$_j$ remains unchanged.

VI. Evaluation

We now evaluate the performance of IAN-CoMP using MATLAB simulation. Due to the diverse implementations of multi-location IAN-CoMP, for simplicity, we only simulate it in Fig. 9 so as to compare with the single-location IAN-CoMP. Without specification, we use IAN-CoMP to denote single-location IAN-CoMP in the following discussion. Fig. 7 compares the proposed scheme with five other algorithms, including ZFBF-CoMP, point-to-point (p2p) MIMO, MIMO broadcast channel (BC) employing DPC and ZF-based precoding respectively, IA-CoMP [10], and Non-CoMP under 2-eNB 2-UE and $N_T=N_R=2$ system settings. For a fair comparison, we set the total system transmit power to $2P_T$, the numbers of antennas at both the transmitter and receiver sides to 4. Specifically, for the implementation of IN, we adjust the signal with a higher channel gain to neutralize the one with a lower gain so as to avoid additional power cost, hence assuring the applicability of IN. In addition, in our simulation, we fix the sum of squares of every two IN precoders' Euclidean norm to 2. As for the cooperative realization of IA, as the discussion below Eq. (18), the square of Euclid norm of each precoder for IA is determined under the constraint of total transmit power $2P_T$ minus the IN's power consumption. We use the general form $[M\ L\ \Delta]$ to denote the parameter settings for different mechanisms, where M is the number of BSs, L is the number of mobile users, and Δ is the total number of data streams that can be served simultaneously for the users. For IAN-CoMP, ZFBF-CoMP, IA-CoMP and Non-CoMP, the transmit power of each eNB is P_T, each UE is equipped with $N_R=2$ antennas, whereas for p2pMIMO and MIMO BC, there is only one BS, and hence its transmit power is $2P_T$. Moreover, for p2pMIMO, only one 4-antenna user is involved, while in MIMO BC there are two 2-antenna users. Note that with generalized parameter settings, not all the above-mentioned schemes are applicable. However, the trend of SE performance with various methods is consistent with that given in Fig. 7. The details can be seen in Figs. 8 and 9.

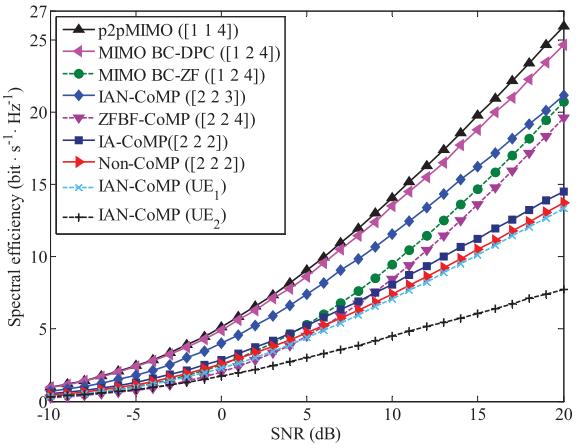

Fig. 7. Spectral efficiency comparison of IAN-CoMP with different mechanisms under $N_T=N_R=2$, $M=2$, and $L=2$.

With p2pMIMO, the precoder and the receive filter are designed based on SVD, with which four orthogonal data streams can be transmitted simultaneously by exploiting spatial multiplexing. This can be regarded equivalent to the case where both eNB and UE sides ideally cooperate. As for MIMO BC, two pre-processing strategies, including DPC and ZF-based precdoing are considered with which CCI can be eliminated and four concurrent data streams are supported. For MIMO BC-DPC, we employ an affine approximation for the sum rate given in [34] as follows:

$$R_{DPC}(\mathbf{H},P_T)\cong LN_R\log_2 P_T-LN_R\log_2 LN_R+\log_2|\mathbf{H}^H\mathbf{H}| \tag{31}$$

where $\cong$ refers to equivalence in the limit, i.e., the difference between both sides converges to zero as $P_T\to\infty$. R_{DPC} is the achievable rate region under the constraints of transmit

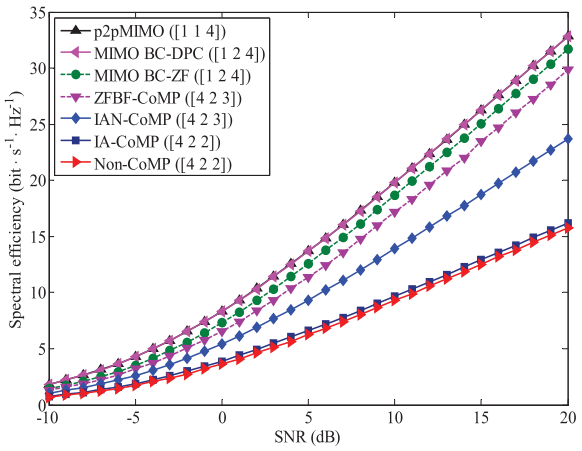

Fig. 8. Spectral efficiency comparison of IAN-CoMP with different mechanisms under $N_T = N_R = 2$, $M = 4$, and $L = 2$.

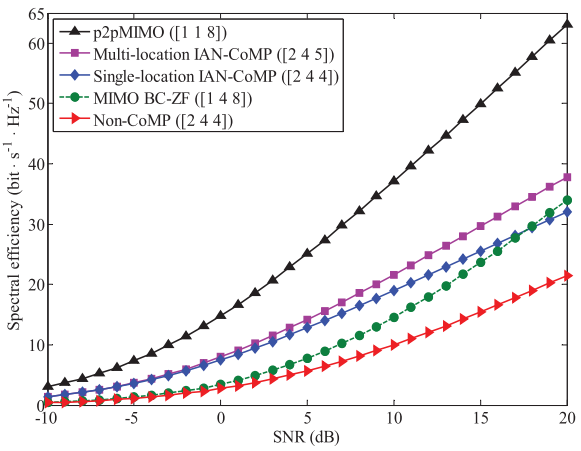

Fig. 9. Spectral efficiency comparison of IAN-CoMP with different mechanisms under $N_T = N_R = 4$, $M = 2$, and $L = 4$.

power P_T and matrix $\mathbf{H}$. $\mathbf{H}$ is the concatenation of the user channel $\mathbf{H}_l$ $(l = 1, 2, \cdots, L)$ and $\mathbf{H}^H = [\mathbf{H}_1^H\ \mathbf{H}_2^H \cdots \mathbf{H}_L^H] \in \mathbb{C}^{N_T \times LN_R}$. L, N_T and N_R represent for the numbers of users and antennas equipped at the transmitter and each user, respectively. As for MIMO BC-ZF, ZF-based precoding is adopted by the BS, and each user implements post-processing independently. With ZFBF-CoMP, complete data information and CSI are shared by eNBs, the pseudo-inverse of the matrix consisting of channels of all scheduled users is adopted as the precoder, and then four data transmissions are available. Essentially, ZFBF-CoMP is the interfering transmitter side implementation. With IA-CoMP, each transmitter can send one data stream to its receiver under the system settings. Receiver nodes decode data successively. The node which recovers its data first will forward the information to the subsequent receivers. However, the receiver side cooperation is required, which is difficult to get in the downlink. For non-CoMP, the SVD-based precoder is employed, the receive filter is designed at each user separately for interference cancellation. Since neither the BS side nor the user side has cooperation capability, each BS serves one user with one data stream, so two streams are supported simultaneously.

As shown in Fig. 7, p2pMIMO achieves the maximum SE, since it is equivalent to the case where both BS and user sides cooperate ideally [22]. MIMO BC is similar to IAN-CoMP in that both schemes are realized based on transmitter-side collaboration and without receiver-side cooperation. Their difference lies in the fact that the degree of the transmitter-side cooperation of the former is higher than that of the later. Hence, sum rate capacity of MIMO BC is a more accurate upper bound for IAN-CoMP compared to p2pMIMO. Moreover, since ZF-based precoding is a linear processing of low complexity but sub-optimal transmission performance, MIMO BC-ZF incurs an absolute rate offset compared to DPC which achieves the sum rate capacity of MIMO BC [34]. Non-CoMP performs poorly. IA-CoMP outperforms Non-CoMP with approximately 1 bit·s^{-1}·Hz^{-1} since it exploits both coordinate transmission and receiver side cooperation. MIMO BC-ZF and ZFBF-CoMP are slightly inferior to non-CoMP in a low SNR region. Since SE is dominated by noise when SNR is low, the influence of CCI is lower than noise power. As a result, signal processing for interference elimination and suppression cannot make an obvious enhancement on the system SE, but on the contrary, effective power loss of the desired signal due to above-mentioned processing deteriorates the SE in the end. As SNR increases, interference gradually becomes the dominant factor limiting SE. Hence, SE of MIMO BC-ZF and ZFBF-CoMP improves significantly over that of non-CoMP, and approaches the proposed IAN-CoMP as SNR grows. With IAN-CoMP, interference cancellation and suppression is implemented while the strength of expected signals is maintained. Consequently, IAN-CoMP outperforms MIMO BC-ZF, ZFBF-CoMP and non-CoMP. SE of both UEs with IAN-CoMP is also plotted in Fig. 7. One can see that UE_1 achieves better transmission than UE_2 since the former is served by two data streams whereas only one is available to the latter.

Fig. 8 plots the SE performance of various schemes under $N_T = N_R = 2$, $M = 4$, and $L = 2$. For a fair comparison, we set the total system transmit power, the numbers of antennas at the transmitter and the receiver side to $2P_T$, 8, and 4, respectively. As shown in the figure, due to the increase of antennas at the transmitter side, SE of all schemes is improved compared to the results given in Fig. 7. SE of MIMO BC-DPC is close to that of the p2pMIMO. For p2pMIMO, MIMO BC and ZFBF-CoMP, all transmit antennas are employed for data sending, i.e., transmit diversity gain is exploited. With IAN-CoMP, each data stream is sent either exclusively by one or collaboratively by two eNBs, whereas for Non-CoMP and IA-CoMP, L out of M eNBs are selected to serve L UEs, i.e., with these methods only a selection diversity gain from multiple eNBs is achieved. As a result, MIMO BC and ZFBF-CoMP outperform IAN-CoMP in SE, and all the three schemes outperform IA-CoMP. Non-CoMP yields the worst SE.

Fig. 9 shows the SE performance of various schemes under $N_T = N_R = 4$, 2 eNBs and 4 UEs. Both single-location and multi-location IAN-CoMP are investigated. The total

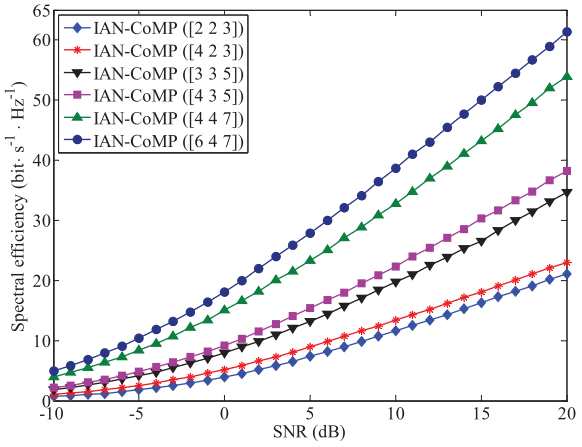

Fig. 10. Spectral efficiency of IAN-CoMP under $M = 2$, $L = 2$, different N_T and N_R.

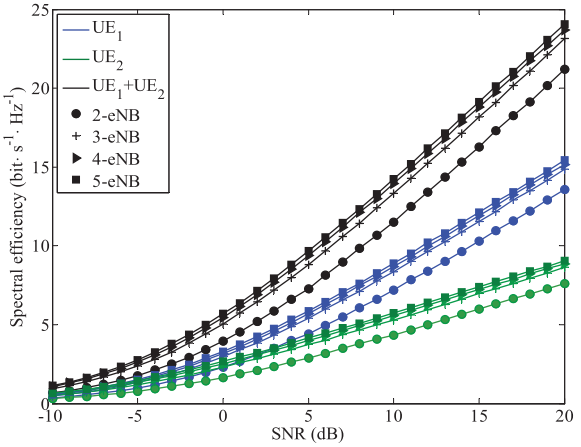

Fig. 11. Spectral efficiency of IAN-CoMP under $N_T = N_R = 2$, $L = 2$, and different Ms.

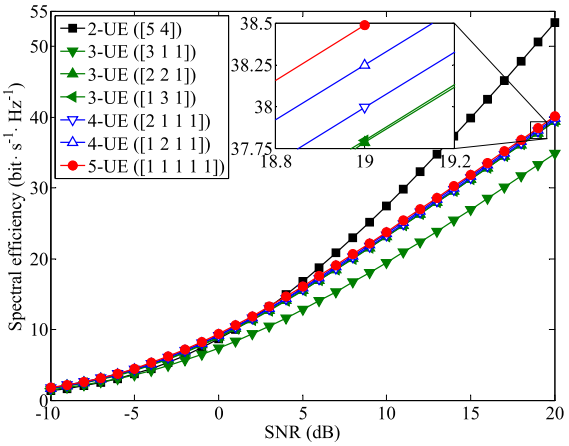

Fig. 12. Spectral efficiency of IAN-CoMP under $N_T = N_R = 5$, $M = 2$, and different Ls.

system transmit power is $2P_T$. The number of antennas at the transmitter and the receiver side are 8 and 16, respectively. Note that the application of Eq. (31) requires $N_T \geq LN_R$ [34], i.e., the aggregate number of receive antennas is no larger than the number of transmit antennas. However, with the above system settings, $N_T \geq LN_R$ doesn't hold, thus in Fig. 9 only MIMO BC-ZF is simulated. Since ZFBF-CoMP requires that the composite channel matrix, consisting of the matrices from all eNB to all UEs, is full row rank, however, under the above system settings, such a requirement cannot be met, incurring unavailability of ZFBF-CoMP. As for IA-CoMP, L eNBs are selected from M candidates, each of them is then used to serve one UE, thus $M \geq L$ should be satisfied. However, in the simulation of Fig. 9, we set $M < L$, thus IA-CoMP is not applicable. As can be seen in the figure, with an increase of N_T, N_R, and L, system SE of all the schemes under study is improved. SE with MIMO BC is inferior to that with single-location IAN-CoMP from low to medium SNR, however, when SNR grows larger than 18dB, MIMO BC excels the single-location IAN-CoMP. This is because with MIMO BC, the maximum number of data streams that the system can simultaneously support is $\min(N_T, LN_R)$, larger than that with single-location IAN-CoMP, however, in order to eliminate CCI, precoding for each stream causes loss of transmission gain, thus, when SNR ranges from low to medium, it is better to employ the DoFs with high transmission gain for data delivery, resulting in high SE of single-location IAN-CoMP compared to MIMO BC, when SNR is large enough, data transmission utilizing all DoFs becomes more efficient, rendering MIMO BC exceeds the proposed single-location IAN-CoMP in SE. As can be seen from the figure, SE of multi-location IAN-CoMP excels that of the single-location one.

Fig. 10 plots the spectral efficiency with proposed IAN-CoMP under different antenna configurations. Let the general form $[N_T \ N_R \ \Delta]$ denote the parameter settings. As shown in the figure, given $N_T \geq N_R$, the achievable SE grows as the number of antennas increases. Provided with fixed N_T (N_R), SE grows as N_R (N_T) increases. Besides, compared to N_T, increasing N_R yields more significant improvements on SE.

Fig. 11 plots the spectral efficiency of IAN-CoMP under $N_T = N_R = 2$, $L = 2$, and different Ms. SEs of both UEs are also illustrated there. Since Δ is irrelevant to M, we simply assign UE$_1$ with two data streams whereas UE$_2$ with one. As shown in the figure, both the system's SE and individual UE's grows with an increase of M, because more selection diversity gain is obtained as the number of eNBs participating in CoMP increases, which is consistent with our theoretical analysis.

Fig. 12 shows the SE performance of the proposed mechanism under different Ls. Based on the analysis in Section IV-C, the number of simultaneously supported users is limited by N_R, however, due to space limitation and hardware cost, mobile terminals cannot be equipped with a large number of antennas. In order to explicitly illustrate the impact of L on SE, we set $N_T = N_R = 5$ and $M = 2$. A general expression $[\delta_1^{max} \ \cdots \ \delta_L^{max}]$ is employed to indicate the allocation of data streams to L users. Note that neutralization of all the UEs' data transmission except for UE$_1$'s is implemented at UE$_1$, whereas for signals carrying UE$_1$'s information IA is achieved at UE$_2$. Since severer CCI is introduced as L grows larger than 2, 2-UE case achieves the highest DoFs, thus outputting the best SE. Given $L > 2$ and the same system DoFs, SE improves with an increase of L since it benefits from

multiple simultaneously-served users. Particularly, when SNR is low, such benefits may outweigh the performance loss due to severer CCI. So, the SE of 4-UE and 5-UE cases slightly outperforms that with 2-UE under small SNR. Note that IN yields less effective signal power loss than IA, resulting in higher SE, e.g., for the three 3-UE cases, the [1 3 1] DoF allocation excels the [2 2 1], and the [2 2 1] outperforms the [3 1 1] case in SE, since 4 data transmissions achieve IN for the former case whereas only 3 and 2 for the latter two cases. To summarize, given $L > 2$ and the same N_R, more users yields larger system SE; while provided with fixed N_R and L, the more signals participating in IN, the higher system SE results.

VII. Conclusion

In this paper, a new CoMP mechanism based on IAN is proposed. By exploiting the BS-side cooperation, transmit precoding and receive filtering are designed jointly. On one hand, IN is used to align two interfering signals carrying the same data in opposite directions in a subspace such that they can be canceled out. On the other hand, IA is applied to align interference signals carrying different information in the same direction in one subspace so as to reduce the dimension of received signal. Based on the cooperative preprocessing at eNBs, ZF is employed at the receiver side to cancel the residual interference and recover the desired information. This scheme is designed first under a specific system configuration, and then extended to more general cases. The proposed IAN-CoMP could achieve effective interference cancellation and suppression by exploiting limited cooperation, hence improving spectral efficiency for cell-edge users significantly.

The number of DoFs of the proposed IAN-CoMP is limited by the CoMP system. By defining average cooperation order for the non-uniform CoMP channel which can subsume the cooperation order defined in [22] as a special case. We have shown that the number of DoFs of IAN-CoMP is limited by the bound provided in [22] given the same number of antennas at both the transmitter and receiver sides. The study of the maximum DoFs of a non-uniform CoMP system with various numbers of transmit and receive antennas can further generalize the study of [22], and hence is of significance. However, this requires significantly more work and beyond the scope of this paper, and we leave it as our future work.

Appendix
Proof of $\lceil \mathcal{B}^* \rceil \geq \left\lfloor \frac{\mathcal{N}-1}{L-1} \right\rfloor$ Under $L \geq 2$

We prove $\lceil \mathcal{B}^* \rceil \geq \left\lfloor \frac{\mathcal{N}-1}{L-1} \right\rfloor$ under $L \geq 3$ and $L = 2$, respectively. For clarity of exposition, we define $\mathcal{G} = \lceil \mathcal{B}^* \rceil - \left\lfloor \frac{\mathcal{N}-1}{L-1} \right\rfloor$. To prove $\lceil \mathcal{B}^* \rceil \geq \left\lfloor \frac{\mathcal{N}-1}{L-1} \right\rfloor$ is equivalent to verifying $\mathcal{G} \geq 0$. As can be easily seen, if we can prove

$$\mathcal{G}^* = \frac{\mathcal{N} + \bar{M}_t + \bar{M}_r - 2}{2} - \frac{\mathcal{N}-1}{L-1} \geq 0, \tag{32}$$

then $\mathcal{G} \geq 0$ follows. By substituting $\bar{M}_r = \frac{1}{L}\left\lfloor \frac{\mathcal{N}-1}{L-1} \right\rfloor$ into Eq. (32), we can have

$$\mathcal{G}^* = \frac{1}{2}\bar{M}_t + \frac{1}{2L}\left\lfloor \frac{\mathcal{N}-1}{L-1} \right\rfloor + \frac{\mathcal{N}-2}{2} - \frac{\mathcal{N}-1}{L-1} \geq 0. \tag{33}$$

By noting that $\left\lfloor \frac{\mathcal{N}-1}{L-1} \right\rfloor \geq \frac{\mathcal{N}-1}{L-1} - 1$, we get

$$\mathcal{G}^* \geq \frac{1}{2}\bar{M}_t + \frac{\mathcal{N}-1}{2L(L-1)} - \frac{1}{2L} + \frac{\mathcal{N}-2}{2} - \frac{\mathcal{N}-1}{L-1}. \tag{34}$$

Then we rewrite (34) as:

$$\mathcal{G}^* \geq \frac{1}{2}\bar{M}_t + \frac{\mathcal{N}L^2 + \mathcal{N} + 3L - 2L^2 - 3\mathcal{N}L}{2L(L-1)}. \tag{35}$$

Since $\frac{1}{2}\bar{M}_t \geq 0$, we then need to prove

$$\frac{\mathcal{N}L^2 + \mathcal{N} + 3L - 2L^2 - 3\mathcal{N}L}{2L(L-1)} \geq 0. \tag{36}$$

For simplicity, we define $\Psi = \mathcal{N}L^2 + \mathcal{N} + 3L - 2L^2 - 3\mathcal{N}L$. Then, to prove (36), we just need to verify $\Psi \geq 0$ under $N_R \geq 2$. First, given $L \geq 5$, inequalities $\frac{1}{3}\mathcal{N}L^2 - 2L^2 > 0$ and $\frac{2}{3}\mathcal{N}L^2 - 3\mathcal{N}L > 0$ hold, and hence $\Psi \geq 0$ follows. Then, by substituting $L = 4$ into Ψ, we have $\Psi|_{L=4} = 20(N_R - 1) > 0$. Moreover, given $L = 3$, we can obtain $\Psi|_{L=3} = 3N_R - 9$, then $\Psi \geq 0$ follows as long as $N_R \geq 3$. At last, we substitute $L = 3$ and $N_R = 2$ into $\lceil \mathcal{B}^* \rceil$ and $\left\lfloor \frac{\mathcal{N}-1}{L-1} \right\rfloor$ to obtain $\lceil \mathcal{B}^* \rceil = \left\lceil 2 + \frac{1}{2}(\bar{M}_t + \bar{M}_r) \right\rceil$ and $\lfloor \frac{5}{2} \rfloor$, and obviously, $\lceil \mathcal{B}^* \rceil > \left\lfloor \frac{\mathcal{N}-1}{L-1} \right\rfloor$ holds. Therefore, $\Psi \geq 0$ under $N_R \geq 2$ is proved, and hence $\lceil \mathcal{B}^* \rceil \geq \left\lfloor \frac{\mathcal{N}-1}{L-1} \right\rfloor$ under $L \geq 3$ follows.

Then we prove $\lceil \mathcal{B}^* \rceil \geq \left\lfloor \frac{\mathcal{N}-1}{L-1} \right\rfloor$ under $L = 2$. Given $L = 2$, the average cooperation order can be computed as $\bar{M}_t = \frac{N_T[2+(2N_R-3)^2]}{N_R(2N_R-1)}$ and $\bar{M}_r = \frac{1}{2}(2N_R - 1)$, and the IAN-CoMP can achieve $2N_R - 1 = \left\lfloor \frac{\mathcal{N}-1}{L-1} \right\rfloor$ DoFs. Recall that the design of IAN-CoMP is under the configuration of $N_T \geq N_R$ and $N_R \geq 2$, thus $\bar{M}_t \geq \frac{2+(2N_R-3)^2}{2N_R-1}$ holds. Then, we can have

$$\lceil \mathcal{B}^* \rceil \geq \left\lceil \frac{2 + (2N_R - 3)^2}{2(2N_R - 1)} + \frac{3}{2}N_R - \frac{5}{4} \right\rceil. \tag{37}$$

Therefore, to prove $\lceil \mathcal{B}^* \rceil \geq \left\lfloor \frac{\mathcal{N}-1}{L-1} \right\rfloor$ under $L = 2$ becomes to verify

$$\frac{2 + (2N_R - 3)^2}{2(2N_R - 1)} + \frac{3}{2}N_R - \frac{5}{4} \geq 2N_R - 1 \tag{38}$$

We rewrite (38) as

$$\frac{2 + (2N_R - 3)^2}{2(2N_R - 1)} - \frac{1}{2}N_R - \frac{1}{4} \geq 0. \tag{39}$$

Since $N_R \geq 2$, $2N_R - 1 > 0$ holds. Then, (39) can be simplified to

$$(N_R - 3)^2 - \frac{13}{4} \geq 0. \tag{40}$$

Obviously, inequality (40) holds as long as $N_R \geq 5$. Moreover, by substituting $N_R \in \{2, 3, 4\}$ into (37) and $2N_R - 1$ respectively, we can find that $\lceil \mathcal{B}^* \rceil \geq 2N_R - 1$ holds. Therefore, $\lceil \mathcal{B}^* \rceil \geq \left\lfloor \frac{\mathcal{N}-1}{L-1} \right\rfloor$ holds for $L = 2$.

Based on the above analysis, we can conclude that given $L \geq 2$, $\lceil \mathcal{B}^* \rceil \geq \left\lfloor \frac{\mathcal{N}-1}{L-1} \right\rfloor$ follows.

REFERENCES

[1] G. Y. Li *et al.*, "Energy-efficient wireless communications: Tutorial, survey, and open issues," *IEEE Wireless Commun.*, vol. 18, no. 6, pp. 28–35, Dec. 2011.

[2] P. Marsch and G. P. Fettweis, *Coordinated Multi-Point in Mobile Communications: From Theory to Practice*. Cambridge, U.K.: Cambridge Univ. Press, 2011.

[3] V. V. Veeravalli and A. El Gamal, *Interference Management in Wireless Networks: Fundamental Bounds and the Role of Cooperation*. Cambridge, U.K.: Cambridge Univ. Press, 2018.

[4] *Further Advancements for E-UTRA, Physical Layer Aspects; Coordinated Multiple Point Transmission and Reception*, document 3GPP TR 36.815, 2010.

[5] W. Liu, S. Han, and C. Yang, "Hybrid cooperative transmission in heterogeneous networks," in *Proc. IEEE 23rd Int. Symp. Pers., Indoor Mobile Radio Commun. (PIMRC)*, Sep. 2012, pp. 921–925.

[6] S. Han, C. Yang, M. Bengtsson, and A. I. Perez-Neira, "Channel norm-based user scheduler in coordinated multi-point systems," in *Proc. IEEE Global Telecommun. Conf. (GLOBECOM)*, Nov./Dec. 2009, pp. 1–5.

[7] Q. Zhang and C. Yang, "Semi-dynamic mode selection in base station cooperative transmission system," in *Proc. IEEE Veh. Technol. Conf. (VTC)*, Sep. 2011, pp. 1–5.

[8] C. M. Yetis, T. Gou, S. A. Jafar, and A. H. Kayran, "On feasibility of interference alignment in MIMO interference networks," *IEEE Trans. Signal Process.*, vol. 58, no. 9, pp. 4771–4782, Sep. 2010.

[9] C. Na, X. Hou, and A. Harada, "Two-cell coordinated transmission scheme based on interference alignment and MU-MIMO beamforming," in *Proc. IEEE 75th Veh. Technol. Conf. (VTC)*, May 2012, pp. 1–5.

[10] S. M. Razavi and T. Ratnarajah, "Interference alignment in partially coordinated multipoint receivers," in *Proc. IEEE 24th Annu. Int. Symp. Pers., Indoor, Mobile Radio Commun. (PIMRC)*, Sep. 2013, pp. 1114–1118.

[11] C. Wilson and V. V. Veeravalli, "Degrees of freedom for the constant MIMO interference channel with CoMP transmission," *IEEE Trans. Commun.*, vol. 62, no. 8, pp. 2894–2904, Aug. 2014.

[12] X. Zhang, M. A. Khojastepour, K. Sundaresan, S. Rangarajan, and K. G. Shin, "Exploiting interference locality in coordinated multi-point transmission systems," in *Proc. IEEE Int. Conf. Commun. (ICC)*, Jun. 2012, pp. 4207–4211.

[13] J. Chen, A. Singh, P. Elia, and R. Knopp, "Interference neutralization for separated multiuser uplink-downlink with distributed relays," in *Proc. Inf. Theory Appl. Workshop (ITA)*, Feb. 2011, pp. 1–9.

[14] T. Gou, S. A. Jafar, C. Wang, S.-W. Jeon, and S.-Y. Chung, "Aligned interference neutralization and the degrees of freedom of the $2 \times 2 \times 2$ interference channel," *IEEE Trans. Inf. Theory*, vol. 58, no. 7, pp. 4381–4395, Jul. 2012.

[15] H. Zeng, X. Yuan, X. Qin, Y. Shi, Y. T. Hou, and W. Lou, "Nullification in the air: Interference neutralization in multi-hop wireless networks," in *Proc. 35th Annu. IEEE Int. Conf. Comput. Commun. (INFOCOM)*, Apr. 2016, pp. 1–9.

[16] D. Wu, C. Yang, and Z. Xiong, "Feasibility of interference neutralization in relay-aided MIMO interference broadcast channel with partial connectivity," in *Proc. IEEE Int. Conf. Acoust., Speech Signal Process. (ICASSP)*, May 2013, pp. 4414–4418.

[17] N. Lee and C. Wang, "Aligned interference neutralization and the degrees of freedom of the two-user wireless networks with an instantaneous relay," *IEEE Trans. Commun.*, vol. 61, no. 9, pp. 3611–3619, Sep. 2013.

[18] Z. K. M. Ho and E. A. Jorswieck, "Instantaneous relaying: Optimal strategies and interference neutralization," *IEEE Trans. Signal Process.*, vol. 60, no. 12, pp. 6655–6668, Dec. 2012.

[19] Z. Li, K. G. Shin, and L. Zhen, "When and how much to neutralize interference?" in *Proc. IEEE Conf. Comput. Commun. (INFOCOM)*, May 2017, pp. 1–9.

[20] R. Wang, X. Yuan, and R. W. Yeung, "MIMO multipair two-way relaying with distributed relays: Joint signal alignment and interference neutralization," *IEEE Trans. Inf. Theory*, vol. 62, no. 3, pp. 1326–1343, Mar. 2016.

[21] Z. Li, S. Cui, K. G. Shin, and J. Gu, "Coordinated multi-point transmissions based on interference alignment and neutralization," in *Proc. 35th Annu. IEEE Int. Conf. Comput. Commun. (INFOCOM)*, Apr. 2016, pp. 1–9.

[22] V. S. Annapureddy, A. El Gamal, and V. V. Veeravalli, "Degrees of freedom of interference channels with CoMP transmission and reception," *IEEE Trans. Inf. Theory*, vol. 58, no. 9, pp. 5740–5760, Sep. 2012.

[23] V. Jungnickel *et al.*, "Backhaul requirements for inter-site cooperation in heterogeneous LTE-Advanced networks," in *Proc. IEEE Int. Conf. Commun. Workshops (ICC)*, Jun. 2013, pp. 905–910.

[24] I. F. Akyildiz, D. M. Gutierrez-Estevez, R. Balakrishnan, and E. Chavarria-Reyes, "LTE-advanced and the evolution to beyond 4G (B4G) systems," *Phys. Commun.*, vol. 10, pp. 31–60, Mar. 2014.

[25] S. Gollakota, S. D. Perli, and D. Katabi, "Interference alignment and cancellation," in *Proc. ACM SIGCOMM Conf. Data Commun.*, Aug. 2009, pp. 159–170.

[26] L. Zhao, S. Biao, and L. Jiandong, "Interference alignment and cancellation based concurrent transmission and scheduling scheme for multi-user CR-MIMO system," *China Commun.*, vol. 10, no. 8, pp. 36–43, Aug. 2013.

[27] S. A. Jafar and S. Shamai (Shitz), "Degrees of freedom region of the MIMO X channel," *IEEE Trans. Inf. Theory*, vol. 54, no. 1, pp. 151–170, Jan. 2008.

[28] M. A. Maddah-Ali, A. S. Motahari, and A. K. Khandani, "Communication over MIMO X channels: Interference alignment, decomposition, and performance analysis," *IEEE Trans. Inf. Theory*, vol. 54, no. 8, pp. 3457–3470, Aug. 2008.

[29] M. A. Maddah-Ali, A. S. Motahari, and A. K. Khandani, "Signaling over MIMO multi-base systems: Combination of multi-access and broadcast schemes," in *Proc. IEEE Int. Symp. Inf. Theory (ISIT)*, Jul. 2006, pp. 2104–2108.

[30] C. Simon and G. Leus, "Round-robin scheduling for orthogonal beamforming with limited feedback," *IEEE Trans. Wireless Commun.*, vol. 10, no. 8, pp. 2486–2496, Aug. 2011.

[31] M. Mehrjoo, M. K. Awad, M. Dianati, and X. S. Shen, "Design of fair weights for heterogeneous traffic scheduling in multichannel wireless networks," *IEEE Trans. Commun.*, vol. 58, no. 10, pp. 2892–2902, Oct. 2010.

[32] G. H. Golub and C. F. Van Loan, *Matrix Computations*, 4th ed. Baltimore, MD, USA: The Johns Hopkins Univ. Press, 2013.

[33] J. H. Lee and W. Choi, "Interference alignment by opportunistic user selection in 3-user MIMO interference channels," in *Proc. IEEE Int. Conf. Commun. (ICC)*, Jun. 2011, pp. 1–5.

[34] J. Lee and N. Jindal, "Dirty paper coding vs. linear precoding for MIMO broadcast channels," in *Proc. IEEE 4th Asilomar Conf. Signals, Syst. Comput. (ACSSC)*, Oct./Nov. 2006, pp. 779–783.

Zhao Li (S'08–M'10) received the B.S. degree in telecommunications engineering and the M.S. and Ph.D. degrees in communication and information systems from Xidian University, Xi'an, China, in 2003, 2006, and 2010, respectively. He was a Visiting Scholar and then a Research Scientist with the Real-Time Computing Laboratory, Department of Electrical Engineering and Computer Science, University of Michigan, from 2013 to 2015. He is currently an Associate Professor with the School of Cyber Engineering, Xidian University. He is also with the Shaanxi Key Laboratory of Information Communication Network and Security, Xi'an University of Posts and Telecommunications, and the School of Information Engineering, Eurasia University. He has published over 40 technical papers at premium international journals and conferences, such as the IEEE TWC, the IEEE INFOCOM, and *Computer Communications*. His research interests include wireless communication, 5G communication systems, resource allocation, interference management, the IoT, and physical layer security.

Jie Chen is currently pursuing the master's degree with the School of Telecommunications Engineering, Xidian University. Her research interests include wireless communication, resource allocation, interference management, and security communication.

Lu Zhen is currently pursuing the master's degree with the School of Telecommunications Engineering, Xidian University. Her research interests include wireless communication, resource allocation, and interference management.

Sha Cui is currently pursuing the master's degree with the School of Telecommunications Engineering, Xidian University. Her research interests include wireless communication, resource allocation, and interference management.

Kang G. Shin (LF'12) received the B.S. degree in electronics engineering from Seoul National University, Seoul, South Korea, and the M.S. and Ph.D. degrees in electrical engineering from Cornell University, Ithaca, NY, USA, in 1970, 1976, and 1978, respectively. He is currently the Kevin and Nancy O'Connor Professor of computer science and the Founding Director of the Real-Time Computing Laboratory, Department of Electrical Engineering and Computer Science, University of Michigan, Ann Arbor, MI, USA. At the University of Michigan, he has supervised the completion of 82 Ph.D. students and also chaired the Computer Science and Engineering Division for three years starting in 1991. From 1978 to 1982, he was with the faculty of the Rensselaer Polytechnic Institute, Troy, NY, USA. He has authored/coauthored more than 900 technical articles (more than 330 of which are published in archival journals) and holds more than 30 patents or invention disclosures. His current research interests focus on QoS-sensitive computing and networks as well as on embedded real-time and cyber-physical systems. He has also received numerous institutional awards and the best paper awards. He is a fellow of ACM.

Jia Liu (S'10–M'12) received the Ph.D. degree from the School of Systems Information Science, Future University Hakodate, Japan, in 2016. He is currently an Assistant Professor with the Center for Cybersecurity Research and Development, National Institute of Informatics, Japan. He has published over 20 technical papers at premium international journals and conferences, such as the IEEE TWC, the IEEE TVT, the IEEE INFOCOM, and *Computer Networks*. His research interests include mobile ad hoc networks, 5G communication systems, D2D communications, the IoT, physical layer security, and cyber security. He was a recipient of the 2016 IEEE Sapporo Section Encouragement Award and the Best Paper Award of NaNA 2017.